
This is the **accepted version** of the journal article:

Sanjuan, Josep; Matamoros, Damià; Casanovas i Vilar, Isaac; [et al.]. «Palaeoecology of Middle Miocene charophytes from the Vallès [U+2012] Penedès and Vilanova basins (Catalonia, Spain)». *Historical biology*, (September 2022). DOI 10.1080/08912963.2022.2106861

This version is available at <https://ddd.uab.cat/record/265986>

under the terms of the  license

1 **Palaeoecology of Middle Miocene charophytes from the Vallès–Penedès**
2 **and Vilanova basins (Catalonia, Spain)**

3 Josep Sanjuan^{1,2*}, Damià Matamoros³, Isaac Casanovas-Vilar⁴, Alba Vicente^{1,2,5}, Josep
4 Anton Moreno-Bedmar⁶, Jonathan Holmes⁷, Carles Martín-Closas^{1,2}

5 ¹ Departament de Dinàmica de la Terra i de l'Oceà, Facultat de Ciències de la Terra,
6 Universitat de Barcelona-UB, 08028 Barcelona, Catalonia (Spain)

7 ² Institut de Recerca de la Biodiversitat (IRBio). Universitat de Barcelona-UB, 08028
8 Barcelona, Catalonia (Spain)

9 ³ Dianastrasse 10a, 9200 Gossau SG, Switzerland

10 ⁴ Institut Català de Paleontologia Miquel Crusafont, Universitat Autònoma de
11 Barcelona, Edifici ICTA-ICP, c/Columnes s/n, Campus de la UAB, 08193 Cerdanyola
12 del Vallès, Barcelona, Catalonia (Spain)

13 ⁵ Instituto Politécnico Nacional. Av. IPN s/N, Col. Playa Palo de Santa Rita. C.P.
14 23096, La Paz, BCS, Mexico

15 ⁶ Instituto de Geología, Universidad Nacional Autónoma de México, Ciudad
16 Universitaria, Coyoacán, 04510, Ciudad de México, Mexico

17 ⁷ Environmental Change Research Centre, Department of Geography, University
18 College London, London WC1E 6BT, United Kingdom

19

20 *Corresponding author: josepsanjuan@ub.edu

21

22 **Abstract**

23 A diverse charophyte assemblage from the Early-Middle Miocene of the Vallès–Penedès
24 and Vilanova basins (Catalonia, NE Spain) is here described and illustrated for the first
25 time. This flora has been recovered from three localities: els Casots (Subirats), Vilobí del
26 Penedès, and Mas de l'Alonso–el Pi Gros (Vilanova i La Geltrú). The charophyte
27 assemblages comprise ten different species distributed among three distinctive aquatic
28 environments, and are approximately simultaneous to major fossil vertebrate sites of these
29 basins. *Sphaerochara ulmensis*, *Chara* cf. *vulgaris*, *Chara molassica* var. *notata*,

30 *Lychnothamnus barbatus* var. *antiquus*, *Lychnothamnus* sp., *Nitellopsis* (*Tectochara*)
31 *merianii*, and *Nitellopsis* sp. occur associated to abraded benthic foraminifera in organic-
32 rich claystones related to palustrine and shallow freshwater coastal lakes.
33 *Lamprothamnium papulosum* forms monospecific assemblages in gypsum-claystone
34 alternations attributed to a coastal brackish water salina. *Chara* cf. *hispidula* and *Chara* sp.
35 are found associated with ostracods in marls and limestones related to a permanent
36 oligohaline and alkaline lake. The discovery of this aquatic flora sheds new light on the
37 palaeoenvironmental conditions that prevailed in the Vallès–Penedès Basin during the
38 Langhian in the context of the Mid-Miocene Climatic Optimum and in the Vilanova Basin
39 during the Serravalian.

40 **Keywords:** Charophyta; Neogene; Aragonian; palaeolimnology; paleolake;
41 palaeoecology

42 **Introduction**

43 In this work we describe three Miocene charophyte assemblages from the Vallès-
44 Penedès and Vilanova i la Geltrú basins (Catalonia), which are near the northeastern coast
45 of Spain.

46 The Vallès–Penedès Basin is one of the best known Miocene basins of eastern Iberia,
47 mostly famous by its dense and continuous land mammal record that comprises hundreds
48 of localities and thousands of specimens (see Casanovas-Vilar et al. 2016a and references
49 therein). A relatively rich fossil pollen and leaf flora has also been documented from this
50 basin (Bessedik 1985; Sanz de Siria Catalán 1993, 1994, respectively), allowing for a
51 comparison with other Southern European floras. Despite its rich continental record, quite
52 surprisingly fossil charophytes have yet to be reported from this area.

53 In the Iberian Peninsula Miocene charophytes have been described in detail from several
54 basins, including the Ebro Basin (e.g., Feist et al. 1994), the Loranca Basin (e.g., Julià de

55 Agar 1991), the Teruel Basin in the Iberian Chain (e.g., Ludwig 1987) and the Portuguese
56 part of the Tagus Basin (Soulié-Märsche 1978). Less remarkable records include the
57 Intermediary Depression in Central Spain (Ortíz et al. 1998), La Cerdanya Basin in the
58 Eastern Pyrenees (e.g., Soulié-Märsche and Martín-Closas 2003) and from the Balearic
59 Islands (Martín-Closas and Ramos 2005). The state of the art about Iberian Miocene
60 charophytes surprisingly contrasts with the lack of charophytes studies from the Vallès–
61 Penedès Basin, and more considering that both land vertebrates and marine mollusks have
62 been thoroughly studied since the late 19th Century.

63 In this work we describe the first fossil charophyte assemblages from the Vallès–Penedès
64 Basin and use them to provide accurate palaeoenvironmental reconstructions of Miocene
65 continental aquatic environments. These derive from three distinct localities, els Casots
66 and Vilobí del Penedès, located in the southern sector (Penedès) of the Basin, and Mas
67 de l’Alonso–el Pi Gros, located in the western sector of the Vilanova i La Geltrú sub-
68 basin (Fig. 1). The els Casots and Vilobí del Penedès localities have been accurately dated
69 by means of bio- and magnetostratigraphy to about 16 Ma (see following section), that is
70 coinciding with the onset of the Miocene Climatic Optimum (MCO). The MCO
71 represented a brief greenhouse interval between ~17 and 15 Ma characterized by an
72 interruption of the Antarctic icesheet build up (Zachos et al. 2001, 2008; Foster et al. 2012)
73 and mid-latitude temperatures as much as 3 °C (You et al. 2009) or even 7 °C
74 (Steinhorsdottir et al. 2020) higher than present. Fossil charophytes from both localities
75 (els Casots and Vilobí del Penedès) not only represent the first charophyte assemblages
76 from the Vallès-Penedès, but also provide new palaeoenvironmental information on
77 continental aquatic environments during the MCO in the western Mediterranean. The
78 sites from the Vilanova Basin i.e. Mas de l’Alonso and el Pi Gros date back to the

79 Serravallian (see below), that is, they postdate the MCO and coincides with a time of
80 gradual cooling (see Zachos et al., 2001, 2008; Steinthorsdottir et al., 2020).

81 The three outcrops studied, els Casots, Vilobí del Penedès and Mas de l'Alonso–el Pi
82 Gros correspond to three different palaeoenvironments, ranging from the late Burdigalian
83 to the Serravalian. They record a diverse charophyte flora and show the potential interest
84 that the study of fossil charophytes has for the understanding of the Vallès–Penedès non-
85 marine palaeoenvironments. The presence of other microfossils (foraminifers and
86 ostracods) provide further information on the palaeoenvironments associated to the
87 charophyte flora.

88 **Geological setting**

89 The Vallès–Penedès Basin is part of a large system of Neogene grabens that mark the
90 present eastern Iberian coastline, continuing further offshore (Roca and Guimerà 1992;
91 Roca et al. 1999; Cabrera et al. 2004). These basins are part of the so-called València
92 Trough which originated because of the opening of the western Mediterranean during the
93 late Oligocene and Miocene (Roca et al. 1999; Roca 2001).

94 The Vallès–Penedès Basin is bounded by NE-SW oriented normal faults that formed after
95 the tectonic inversion of ancient alpine compressional structures during the late Oligocene
96 to Early Miocene (Fontboté 1954; Roca and Guimerà 1992). These limit the basin, which
97 is 100 km long by 12-14 km wide, with the surrounding horsts of the Catalan Litoral
98 Ranges. The Vallès-Penedès main fault is located in its northwestern margin, where the
99 basement is attained at up to 4000 m depth (Bartrina et al. 1992; Roca et al. 1999). Basin
100 basement, and corresponding sediment thickness, gently grades far away from the active
101 margin towards the southeastern margin of the basin to just a few meters (Cabrera et al.
102 1991). The southwestern margin of the basin is only affected by minor faults which were
103 overlapped by Early to Middle Miocene sedimentary sequences (Cabrera 1981a; Cabrera

104 and Calvet 1996). These were later fractured as result of minor fault reactivations
105 (Cabrera 1981a; Cabrera and Calvet 1996). The basin is divided into two distinct sectors
106 or sub-basins, Vallès and Penedès, by the NW-SE oriented Llobregat fault (Fontboté
107 1954; Cabrera and Calvet 1996). The semi-graben also shows a strong internal
108 compartmentation due to the occurrence of small horsts and grabens, broadly parallel to
109 the main fault (Permanyer 1990; Cabrera and Calvet 1996).

110 The Miocene record of the Vallès-Penedès basin has been subdivided into four main
111 lithostratigraphic units which have been dated combining bio- and magnetostratigraphy
112 (Agustí et al. 1985; Cabrera and Calvet 1996; Cabrera et al. 1991; Casanovas-Vilar et al.
113 2016b; de Gibert and Casanovas-Vilar 2011):

114 (1) Basal Breccia Unit. This consists of monogenic conglomerates and breccias and crops
115 out only at a few points in the Garraf-Montnegre horst. It dates back to the Ramblian
116 mammal age (early Burdigalian) in the Vallès sector and it is younger in the Penedès,
117 dating back to the early Aragonian (late Burdigalian and earliest Langhian; de Gibert and
118 Casanovas-Vilar 2011; Casanovas-Vilar et al. 2022).

119 (2) Lower Continental Units. Consist of alluvial fan red beds, including conglomerates,
120 sandstones, and siltstones. Older alluvial fan deposits within this unit were sourced from
121 the southeastern basin margin, while younger ones were also sourced from the
122 northwestern reliefs and expanded in the lowlands covering wider areas. Shallow
123 carbonate and evaporite lacustrine systems developed in zones of the southeastern part of
124 the basin (Cabrera et al. 1979; Cabrera 1981a, b), such as the Subirats detritic-carbonatic
125 system, which includes the site of els Casots (see Casanovas-Vilar et al. 2022). This unit
126 mainly covers the Burdigalian (Early Miocene) and coincides with the rifting phase in the
127 Vallès–Penedès Basin (Cabrera et al. 2004). The els Casots site has been dated to the
128 earliest Langhian (15.9 Ma).

129 (3) The Marine and Transitional Units. These developed during the late Burdigalian to
130 the early Serravallian and were related to a global sea-level rise that took place in the
131 context of the MCO between 17 and 15 Ma (Miller et al. 2020). These also coincide with
132 the beginning of the post-rift phase, when the faults that bounded the southeastern margin
133 of the basin became inactive and were overlapped and overlapped by the sedimentary infill
134 (Cabrera and Calvet 1996; Cabrera et al. 1991, 2004; Roca et al. 1999). At least three
135 episodes of marine transgression and regression are recorded in the basin: late
136 Burdigalian, Langhian and early Serravallian (Cabrera et al. 1991; Cabrera and Calvet
137 1996; Roca et al. 1999; de Gibert and Casanovas-Vilar 2011; Casanovas-Vilar et al.
138 2016b). Coastal saline lakes (sabkhas) developed just below the marine units in the area
139 of Vilobí del Penedès, which represents a lifted block of the basin basement (Permanyer
140 1990). A diverse set of gypsum deposits up to 60 m thick developed in these sabkhas (Ortí
141 and Pueyo 1976; Agustí et al. 1990). These gypsum deposits are overlain by claystones,
142 which have yielded various charophyte assemblages, that are ultimately covered by
143 oyster-rich greyish claystones and bioclastic limestones corresponding to the Langhian
144 transgression. The gypsum units have been generally correlated to the late Burdigalian
145 (Ortí and Pueyo 1976; Agustí et al. 1990; de Gibert and Casanovas-Vilar 2011), while the
146 overlying claystones, which include small mammal fossils, indicate a younger, earliest
147 Langhian, age (Jovells-Vaqué, 2020).

148 (3) Upper Continental Units. These cover the Serravallian and Tortonian and represent the
149 late post-rift phase in the basin (Cabrera et al. 2004). They consist of alluvial fan deposits
150 that were sourced from the reliefs in the northwestern margin while the Vallès-Penedès
151 main fault remained active (Agustí et al. 1985, 1997; Cabrera and Calvet 1996; Roca et
152 al. 1999; Casanovas-Vilar et al. 2016a, b; de Gibert and Casanovas-Vilar 2011). Most of
153 the fossil vertebrate sites of the Vallès-Penedès Basin are located in the distal to marginal

154 facies of alluvial fan systems (Casanovas-Vilar et al. 2016 a, b), but this unit has not
155 yielded charophyte localities thus far.

156 There are several smaller grabens next to the coast, south of the Garraf-Montnegre horst
157 of the Catalan Coastal Ranges. These include the Pla de Barcelona, Baix Llobregat, Sant
158 Andreu de la Barca, Olesa de Bonesvalls and Vilanova basins, and all formed in the
159 context of the same extensional processes that originated the Vallès-Penedès Basin.

160 The Vilanova basin is about 5 km wide by 11 km long (Fig. 1). Same as the Vallès-
161 Penedès, its northwestern margin is limited by a major normal fault affecting the pre-
162 Miocene basement, while the southeastern margin is defined by minor normal faults that
163 are overlapped by Quaternary sediments or are currently under sea in most of the basin
164 (Ramos-Guerrero et al. 1996). Ramos-Guerrero et al. (1996) defined up to four
165 lithostratigraphic units attaining a maximum thickness of about 400 m. The oldest unit
166 (M0) is represented by the marginal complex (breccias) associated and genetically related
167 to the main faults that bound the basin. The other three units show a vertical evolution
168 from continental alluvial environments at the base (M1), freshwater and brackishwater
169 lacustrine facies (M2), to marine (littoral and restricted shelf-bay) at the top (M3). The
170 charophyte assemblages studied here (localities of Mas de l'Alonso and el Pi Gros) have
171 been recovered from the M2 unit (Intermediate Detrital-Carbonate Unit) which is mainly
172 composed of lacustrine marls and limestones. These lithostratigraphic units have been
173 correlated to the Serravallian, although the lowermost alluvial conglomeratic units may
174 correspond to Langhian (Cabrera et al. 2004).

175 -----Figure 1 near here-----

176

177 **Materials and methods**

178 The fossil flora herein studied has been recovered from soft rocks (claystones and marls)
179 from three distinct localities: els Casots, Vilobí del Penedès, in the Penedès sub-basin and
180 Mas de l'Alonso–el Pi Gros, in the Vilanova i la Geltrú sub-basin (Fig. 1). The
181 coordinates of these localities are: els Casots (Subirats), 41°24'56.57"N 01°48'41.78"E;
182 Vilobí del Penedès, 41°23'15.24"N, 01°39'10.90"E; Mas de l'Alonso (Vilanova i la
183 Geltrú), 41°14'57.28"N, 1°43'39.59"E, and el Pí Gros (Vilanova i la Geltrú),
184 41°14'52.57"N, 01°42'50.09"E.

185 In total, 12 samples of 2 kg each one were treated to extract the microfossils. Samples
186 were disaggregated in water, hydroxide peroxide and sodium carbonate and later wet-
187 sieved using sieves with mesh apertures of 1, 0.5, and 0.3 mm. In case of Vilobí del
188 Penedès (sample V6/7), about 2000 kg of sediments were screen-washed during a field
189 campaign undertaken by the Institut Català de Paleontologia (ICP) in the 1990s. The field
190 campaign focused on the recovery of microvertebrate remains and the smallest mesh
191 aperture used during the sieving process was 0.5 mm. In April 2021, 2 kg of sediments
192 were taken from the same outcrop to recover a smaller microfossil fraction (200 – 500
193 µm), which was lost in the previous campaign because a larger mesh size was used.

194 Nine out of the twelve studied samples yielded microfossils including gyrogonites,
195 ostracod carapaces, skeletons of foraminifera, and fish teeth (Fig. 2). Microfossils were
196 sorted after inspecting the residue washed sediment under a light microscope. Selected
197 gyrogonites were measured using the software Motic Images Plus 2.0 ML in a
198 stereomicroscope Motic BA310 with a built-in digital camera housed in the Departament
199 de Dinàmica de la Terra i de l'Oceà (Facultat de Ciències de la Terra), Universitat de
200 Barcelona). The biometric parameters considered were the gyrogonite height (µm), the
201 gyrogonite width (µm), the number of spiral turns observed in lateral view and the
202 isopolarity index (gyrogonite height/gyrogonite width × 100). Well-preserved

203 microfossils were selected and photographed using the scanning electronic microscope
204 (SEM) QUANTA 200 located at the Centres Científics i Tecnològics, Universitat de
205 Barcelona (CCiTUB). Thin-sections, ca. 30 µm in thickness, were prepared from four
206 limestone beds from els Casots and Mas de l'Alonso-el Pi Gros localities (Fig. 2). The
207 microfossils illustrated herein are curated at the Institut Català de Paleontologia Miquel
208 Crusafont (ICP) at Sabadell (Catalonia, Spain) with catalogue numbers IPS122528,
209 IPS122530 and IPS127514 to IPS127517.

210 **Results**

211 *Depositional setting and age*

212 *Els Casots (Subirats)*

213 Els Casots is a key vertebrate fossil site situated in the municipality of Subirats, in the
214 south-western margin of the Penedès sub-basin (Fig. 1). The Miocene succession at els
215 Casots area directly overlies the basement, which consists of Mesozoic (mainly Early
216 Cretaceous) marine carbonates (Casanovas-Vilar et al. 2022). The Miocene succession
217 was studied by means of geological core sampling and is described in detail in Casanovas-
218 Vilar et al. (2022). The core records a basal breccia followed by a 25 m-thick, cyclically-
219 arranged mudstone/limestone succession that at the bottom includes thin (mm to dm
220 thick) sub-bituminous coal deposits. The upper part of the cycle is a carbonate term that
221 includes a variety of bioclastic- to micrite-dominated limestones that range from a few
222 centimetres to a maximum of a couple of meters thick. The carbonate facies include
223 bioclastic laminae alternated with very thin tufa-like carbonates (Cabrera 1979). Thin
224 ferruginous laminae are associated to some of the bioclastic facies. Both carbonates and
225 siliciclastic mudstones may include abundant plant fragments and freshwater gastropod
226 shells or casts. The stratigraphic succession indicates lacustrine to palustrine
227 environments with cyclically oscillating water level. This lacustrine/marshy succession

228 has yielded abundant and remarkably complete terrestrial vertebrate fossils in the
229 excavated area of the site. The vertebrate fauna comprises up to 75 different vertebrate
230 species including amphibians, reptiles, birds and mostly mammals. The finding of several
231 articulated partial skeletons indicate that the site records an autochthonous to
232 parautochthonous vertebrate assemblage (Casanovas-Vilar et al. 2022). The charophyte
233 flora studied here was recovered from a 3.5 m thick section laterally equivalent to the
234 vertebrate-bearing lacustrine/marshy layers (samples C1-C4 in Fig. 2). This consists of
235 organic-rich claystones alternated with marls and a limestone bed (Figs 2 and 3A–B).
236 Claystone beds range from 10 to 50 cm thick and show strong color variation from
237 yellowish, gray to dark gray (Figs 2 and 3A–B). Some organic-rich claystones have
238 yielded abundant plant remains such as leaf fragments of helophytic plants, e.g., *Typha*,
239 well-preserved charophyte gyrogonites, abraded benthic foraminifera, plus vertebrate
240 bones, sometimes in anatomical connection. Some claystone intervals present root marks.
241 In some horizons abundant and irregular carbonate nodules occur (Fig. 3A). A 20 cm
242 thick limestone bed with packstone texture includes mollusk shell fragments, 150 µm thin
243 carbonate planar crusts (Fig. 3C-H) and oncoids (Fig. 3G), both interpreted as of
244 cyanobacterial origin.

245 Claystones at els Casots are attributed to deposition in a quiet and shallow lake. The
246 presence of nodular carbonates, mottling and root marks suggests that the original
247 lacustrine sediments were subject to fluctuations of the water table leading eventually to
248 subaerial exposure with a development of pedogenetic features, similar to those described
249 elsewhere by Alonso-Zarza and Wright (2010) and references herein. Limited oxygen
250 levels and rapid burial at the lake margins favored the preservation of mammal remains
251 and helophytic plant leaves found in darker claystone intervals. Charophytes from these
252 claystones grew under shallow lake conditions, while abraded remains of foraminifera

253 were probably whased in from nearby marine settings. The limestone layer studied at els
254 Casots is interpreted as deposited in a shallow pond. The occurrence of oncoids and
255 abundant mollusk-shell fragments suggest that higher hydrodynamic conditions and
256 perhaps trampling prevailed during its deposition. Moreover, the abundance of
257 cyanobacterial crusts and absence of charophyte remains in the same limestone bed
258 suggest that the water was eutrophic (Martín-Closas, 1999).

259 The lacustrine succession at els Casots ends rather abruptly and is followed by
260 reddish and mottled mudstones and sandstones that record subaerial distal channelized
261 alluvial fan facies. The continental deposits are in turn overlain by an oyster coquina and
262 a bioclastic quartzarenite, which marks the early Langhian transgressive surface in this
263 sector of the Vallès-Penedès Basin.

264 The age of els Casots is well constrained thanks to bio- and magnetostratigraphic
265 data (see Casanovas-Vilar et al. 2022). For a long time, this site was correlated to the
266 latest Early Miocene European mammal Neogene zone MN4, but the recent data indicate
267 a correlation to Aragonian subzone Cb, which corresponds to the earliest MN5.
268 Magnetostratigraphic data from the 30-m-thick els Casots succession indicate reverse
269 polarity which, coupled with the correlation to Aragonian subzone Cb (16.15–15.94 Ma;
270 boundaries after Van der Meulen et al. 2012), results in an estimated age of ~15.9 Ma for
271 the site of els Casots. Therefore, els Casots would coincides with the onset of the Miocene
272 Climatic Optimum (Zachos et al. 2001, 2008; Holbourn et al. 2015). Overall,
273 sedimentological, palaeobotanical (scarce macroflora remains) and faunal data indicate
274 that els Casots corresponds to an ancient freshwater lacustrine or palustrine environment
275 that developed in a tropical-subtropical climate with rainfall seasonality (Casanovas-Vilar
276 et al. 2022).

277

278 -----Figure 2 near here-----

279

280 -----Figure 3 near here-----

281

282

283 -----Figure 4 near here-----

284

285 *Vilobí del Penedès*

286 The section studied at Vilobí del Penedès overlies unconformably the Cretaceous
287 limestone substrate (Fig. 1). The base of the sequence is represented by non-marine
288 breccias, detritic red beds and limestones of the Lower Continental System, which in turn
289 are overlain by a 60 m thick evaporitic sequence mainly composed of secondary gypsum
290 but showing primary gypsarenite at the top (Ortí and Pueyo 1976; Ortí 1990). The
291 succession follows with a 7-m-thick interval dominated by reddish and grey claystones
292 which have yielded the charophyte flora studied herein (samples V1-V6/7 in Fig. 2.2) and
293 micromammal remains that had been previously attributed to the early Aragonian, MN4
294 zone, corresponding to the latest Early Miocene (Agustí et al. 1985, 1990; Casanovas-
295 Vilar et al. 2016a). However, the rodent fauna includes the same cricetid species recorded
296 at els Casots (Jovells-Vaqué and Casanovas-Vilar 2021) and amongst the eomyids only
297 the species *Ligerimys ellipticus* is present (Jovells-Vaquè 2020). Consequently, this
298 favors a correlation with Aragonian subzone Cb and indicate an early Middle Miocene
299 age (MN5) for the site instead (Jovells-Vaqué 2020). Therefore, it would be
300 chronologically very close to other sites of the Vallès-Penedès Basin immediately before

301 the Langhian regional marine transgression, such as els Casots or Sant Mamet (Sant Cugat
302 del Vallès).

303 The upper part of the Vilobí del Penedès succession, which has been studied here in more
304 detail, can be subdivided into three intervals. The first one is 2.5 m thick and overlies a
305 laminated gypsarenite (Fig. 4A). It is composed of an alternation of primary gypsum and
306 greenish claystones rich in charophytes and ostracods. Up to 4 parasequences of gypsum-
307 claystone alternations can be distinguished (Fig. 4B). A semi covered greenish claystone
308 bed, 1.5 m thick, lays over the gypsum-claystone alternation and yielded a second,
309 species-rich charophyte assemblage (Fig. 4C). The second interval is represented by 2.5
310 m of reddish claystone covered by an oyster bank that marks the base of the third interval
311 (Fig. 4D), which is dominated by grey marls and bioclastic limestones rich in marine
312 fossils such as echinoderms and coralline rhodophytes.

313 The evaporitic succession at Vilobí del Penedès has been interpreted by Bitzer (2004) and
314 references therein as having been deposited in a restricted coastal lake or salina (sabkha).

315 The facies alternation of gypsum and claystone horizons with charophytes observed
316 above the evaporitic unit, suggests that sediments settled under fluctuating salinity
317 conditions within the coastal salina. Gypsum layers precipitated in hypersaline
318 conditions, of up to 110‰ according to Bitzer (2004), while claystone layers were
319 deposited in more diluted conditions, corresponding to brackish water, as shown herein.

320 Each gypsum-claystone parasequence can be interpreted as small transgressive-regressive
321 cycle within the salina (Fig. 2). The absence of evaporites and the presence of a diverse
322 charophyte assemblage in the overlying grey claystone beds indicate that diluted
323 conditions finally prevailed, corresponding probably to a coastal freshwater lake (Fig.
324 4C). Finally, the oyster bank and the bioclastic limestone located atop of the section marks
325 the onset of the Langhian regional marine transgression (Fig. 4D).

326 *Mas de l'Alonso–el Pi Gros (Vilanova i la Geltrú):*

327 The studied succession is located at the western margin of the Vilanova i la Geltrú basin
328 (Fig. 1) and corresponds to the Intermediate Detrital-Carbonate Unit (M2) of Ramos-
329 Guerrero et al. (1996). The outcrop at Mas de l'Alonso consists of dark grey organic-rich
330 claystones with charophytes topped by a metric yellowish lacustrine limestone bed (Fig.
331 2.4). Two samples provided charophytes (samples MA1 and MA2 in Fig. 2.4). About 1
332 km westwards, at the el Pi Gros locality, a lateral equivalent of the same non-marine
333 sequence crops out and shows a 3.5 m succession of yellowish limestone alternated with
334 marls, claystones, and siltstones (Figs 2.3 and 5). Four horizons yielded charophytes, i.e.,
335 samples PG1-PG4 in Fig. 2.3. Light grey to yellowish limestone beds at the base of the
336 el Pi Gros section range in thickness from 10 to 30 cm. They display wackstone-packstone
337 textures and contain abundant microfossils such as ostracods and gyrogonites (Fig. 5C–
338 H). These limestones are overlain by two parasequences of limestone beds with
339 stromatolithic lamination covered by reddish bioturbated claystones (Figs 2.3 and 5B).
340 The upper part of the section at el Pi Gros shows 0.5 m-thick cross-bedded calcarenite
341 and is topped by a 0.6 m limestone bed displaying packstone textures rich in gyrogonites,
342 charophyte thalli, dasycladaleans, ostracods, and potamidid gastropods (Fig. 2.3). Above
343 these materials marine facies of the M3 Unit of Ramos-Guerrero et al. (1996) crop out.
344 Despite some authors suggested that the M2 unit is Langhian in age (Batllori and Moreno
345 2003), the micromammals from fossil sites located within this unit indicate younger ages
346 (Serravalian). The site of los Viñedos (Sant Pere de Ribes), yielded small vertebrate
347 remains that are succinctly reported in Ramos-Guerrero et al. (1996). The revised faunal
348 list includes the cricetids *Megacricetodon crusafonti* and *Hispanomys* cf. *decedens* which
349 would indicate a correlation with the *Megacricetodon crusafonti* + *Democricetodon*
350 *larteti* Concurrent Range Subzone of the Vallès-Penedès Basin (Casanovas-Vilar et al.

2016b), thus indicating an age closer to 12.4–12.5 Ma, that is late Aragonian (chronologically equivalent to the late Serravallian). A second site, Sant Pere de Ribes 1, located at the Can Mestre quarry (Ramos-Guerrero et al. 1996), has yielded additional small mammal remains. These include just a few teeth that are assigned to *Democricetodon crusafonti* (referred to as *Renzimys bilobatus* in Ramos-Guerrero et al. 1996) a species that is first recorded during the late Aragonian in the Vallès-Penedès at 11.88 Ma (Casanovas-Vilar et al. 2016b) and slightly earlier (12.4 Ma) in the Calatayud-Montalbán Basin (Aragon; Van Dam et al. 2014). Therefore, unit M3 would belong to the late Serravallian as well.

According to Ramos-Guerrero et al. (1996), the sequence integrating the M2 and M3 units grades upwards from lacustrine to brackish and finally marine environments. The lacustrine conditions of Unit M2 were inferred because of the presence of freshwater gastropods, helophytic plant stems, and charophyte remains (Batllori and Moreno 2003 and references therein). The locality of el Pi Gros is well known by the diverse and rich mollusk fauna preserved as molds, and the bioerosion ichnofossils, both found in the overlying marine M3 Unit (Batllori and Moreno 2003; Belaústegui et al. 2018). In contrast, the fossils of the M2 Unit are poorly known.

Microfossils recovered from the lower marls at Mas de l'Alonso (sample MA-1, Fig. 3 and Table 1) and el Pi Gros (sample PG-2, Fig. 3, Table 1) are well preserved and do not show signs of fragmentation or abrasion. Moreover, ostracod carapaces frequently appear with the two valves articulated suggesting that they were buried *in situ*. The absence of charophyte thalli in these marls suggest that there was a certain selection of the original plant remains, and that gyrogonites may have been laterally transported from the shallower areas of the lake where they grew. The occurrence of rare and abraded foraminifera at Mas de l'Alonso is interpreted as result of transport from a nearby marine

376 coastal area. Altogether these data suggest that the depositional environment of these
377 marls corresponded to a relatively deeper part of a freshwater lake. The overlying
378 charophyte-rich limestones were deposited in shallower freshwater environments, where
379 lime-producing organisms thrived. Wackestone–packstone textures suggest the
380 prevalence of sublittoral lacustrine conditions (e.g., Gierlowski-Kordesch 2010). Higher
381 in the series, the substitution of charophyte-rich marl and limestones by stromatolite
382 limestones and reddish claystone suggest that palaeoenvironmental conditions changed,
383 difficulting the growth of charophytes. The occurrence of the terrigenous red claystone
384 atop of the stromatolite, probably indicating deposition in a floodplain, suggest that the
385 nutrient input to the lake may have increased during the development of stromatolites,
386 hindering the development of charophytes.

387

388 -----Figure 5 near here-----

389

390 **Systematic palaeobotany (Charophytes)**

391 Division Charophyta Migula, 1897

392 Class Charophyceae Smith, 1938

393 Order Charales Lindley, 1836

394 Family Characeae Richard ex C. Agardh, 1824

395 Subfamily Nitelloideae A. Braun in Migula, 1897

396 Genus *Sphaerochara* (Mädler, 1952) emend. Soulié-Märsche, 1989

397 *Sphaerochara ulmensis* (Straub, 1952) comb. nov. Grambast, 1962

398 Fig. 6A–I

399 1952. *Chara ulmensis* Straub, p. 470, pl. A, fig. 19.

400 1962. *Sphaerochara ulmensis* Grambast, p. 77.

401 *Material:* This species occurs at Vilobí del Penedès and Mas de l'Alonso–el Pi Gros
402 (Table 1). Twenty-three gyrogonites were measured in sample MA1 and nine specimens
403 in sample V6/7 (Table 2 in supplementary data).

404 *Description:* Gyrogonites from MA1 are small, 398–477 μm high (mean 437 μm) and
405 330–431 μm wide (mean 391 μm), prolate spheroidal in shape, with an isopolarity index
406 of 112 (mean). Nine to ten spiral turns are visible in lateral view. Spiral cells are 53 μm
407 high in average and ornamented with an irregular mid-cellular crest (Fig. 6F–H). The
408 thickness of the mid-cellular crest can vary significantly, and it can stretch the complete
409 width of the spiral cell (Fig. 6B, C and C–E). The apex is rounded in lateral view. The
410 apical end of each spiral cell is ornamented with a small, individualized coma-shaped
411 nodule (Fig. 6A). The basal plate is visible from the outside and it is located within a large
412 pentagonal basal pore of ~ 75 μm across (Fig. 6D and I). The external part of the basal
413 plate bears a central nodule (Fig. 6D and I). Gyrogonites from the sample V6/7 at Vilobí
414 del Penedés (Fig. 6A–D) are ~ 175 μm larger and wider than specimens extracted from
415 Mas de l'Alonso.

416 *Remarks:* This species shows strong morphological similarities to other ornamented
417 *Sphaerochara* gyrogonites from the European Paleogene displaying mid-cellular crests
418 such as *S. hirmeri* (Rasky 1945) Mädlar 1952 and *S. labellata* Feist and Ringede 1977.
419 Gyrogonites of *S. ulmensis* are longer and show a higher ISI index than the two
420 aforementioned taxa. Moreover, this species displays a thicker and more prominent mid-
421 cellular crest. The subtle differences between these three coeval ornamented
422 *Sphaerochara* species suggest that a comprehensive taxonomic revision should be
423 conducted in future studies.

424 *Fossil record and distribution:* This taxon has been reported in several Paleogene and
425 Neogene basins worldwide i.e., Europe, Middle East, and China mainly in sedimentary
426 sequences ranging in age from the upper Rupelian (early Oligocene) to the Tortonian
427 (Late Miocene). In Europe it is reported from several basins such as the Rhine Graben in
428 North and Central Germany (Straub 1952; Schwarz 1997 and references therein); the
429 Alpine Molasse in South Germany (Mädler 1955; Horn af Rantzien, 1959; Reichenbacher
430 and Schwarz 1997); the Provence (Feist-Castel 1977), and the Languedoc, both in France
431 (Chellai et al. 1982); the Ebro Basin in Catalonia (Feist et al. 1994); and the Cluj Basin
432 in Romania (Baciu and Feist 1999). *S. ulmensis* has also been reported by Mädler and
433 Staesche (1979) from several basins of Central Anatolia (Turkey), and Knobloch (1979)
434 further recovered *S. ulmensis* in Neogene rocks from Iraq. In China, *S. ulmensis* is found
435 in Oligocene deposits from the Bohai coastal region (Xinlun 1978) as well as in several
436 Chinese provinces, such as Sichuan (Huang et al. 1988), Yunnan (Liu 1989), Xinjiang
437 (Lu and Luo 1990) and Qinghai (Tang and Di 1991).

438 *Palaeoecology:* *S. ulmensis* is found in limestones attributed to well-developed lacustrine
439 systems, e.g., the Trévaresse limestone Formation in Aix-en-Provence, France (Feist-
440 Castel 1977). Based on the associated microfossils, Reichenbacher and Schwarz (1997)
441 concluded that *S. ulmensis* was a halophobous taxon, adapted exclusively to freshwater
442 habitats.

443 Subfamily Charoideae A. Braun in Migula 1897

444 Genus *Chara* Linnæus, 1753

445 *Chara* cf. *vulgaris* Linnæus, 1753

446 Fig. 6 J–N

447 1753. *Chara vulgaris* Linnæus, p. 1156

448 1989. *Chara vulgaris* var. *vulgaris* Soulié-Märsche, p. 97, pl. 22

449 *Material:* This taxon dominates the flora in the sample C4 from els Casots (Table 1). Fifty
450 gyrogonites were measured (Table 2 in supplementary data).

451 *Description:* Gyrogonites are of medium size, 378–584 μm high (mean 466 μm) and 256–
452 430 μm wide (mean 352 μm), showing a prolate to perprolate shape and an isopolarity
453 index ranging between 112 and 166 (mean 133). Ten to thirteen (mainly eleven)
454 convolutions are visible in lateral view (Fig. 6K–M). Spiral cells are flat to concave, non-
455 ornamented and ~ 44 μm in height. Spiral cells expand at the apical area (Fig. 6J) forming
456 a psilocharoid apex type (Feist et al. 2005). The base is rounded or slightly pointed
457 showing a small pentagonal basal pore of ~ 48 μm in diameter (Fig. 6N).

458 *Remarks:* The population described herein is remarkably similar to gyrogonites of living
459 *C. vulgaris* in morphological characters such as the apical and basal structure, gyrogonite
460 width and convolution number in lateral view (Soulié-Märsché 1989; Sanjuan et al.
461 2017). However, the studied fossil sample shows gyrogonite heights ~ 100 – 150 μm
462 shorter than living populations.

463 *Fossil record and distribution:* Fossils of *C. vulgaris* are poorly known in Neogene
464 sedimentary sequences. Ghetti et al. (2002) reported gyrogonites of *C. vulgaris* from Late
465 Miocene (early Messinian) rocks of the Velona Basin (Siena, Central Italy). Bathia et al.
466 (1998) found this species in the Plio-Pleistocene intermountainous Himalayan basins
467 (Kashmir, India). Fan et al. (1996) also recovered gyrogonites attributed to this taxon in
468 upper Pleistocene lacustrine facies in the Bangong Co Basin (Western Tibet). Large
469 samples of *C. vulgaris* were recovered by Soulié-Märsche (1991) and Soulié-Märsche et
470 al. (2010) from Pleistocene/Holocene paleolakes from Chad, Algeria and Sudan (Africa).

471 *Palaeoecology: Chara vulgaris* thrives in many kinds of shallow non-marine waterbodies
472 worldwide (Corillion 1972). This taxon grows in temporary ponds or permanent lakes
473 from the depth of several centimeters to up to 1 m (Krause 1997). It can live in freshwater
474 to oligohaline conditions, but calcified gyrogonites are only formed at salinities below 5
475 ‰ and in alkaline water (Ghetti et al. 2002 and references therein). It has also a wide
476 tolerance to different trophic conditions including eutrophic water (Korsch 2016).

477

478 *Chara molassica* var. *notata* (Straub, 1952) comb. nov. Soulié-Märsche, 1989

479 Fig. 6O–U

480 1952. *Chara molassica* forma a Straub, p. 467, pl. A, fig. 4–5

481 1965. *Chara notata* Grambast and Paul, p. 245

482 1989. *Chara molassica* var. *notata* Soulié-Märsche, p. 146

483 *Material:* Fifty specimens were extracted from Vilobí del Penedès and fifteen gyrogonites
484 from els Casots (Table 1). Thirty-five specimens were measured from the sample V6/7
485 (Table 2 in supplementary data).

486 *Description:* Gyrogonites are of medium size, 498–599 µm high (mean 520 µm) and 320–
487 416 µm wide (mean 377 µm). They are subprolate in shape and display a wide isopolarity
488 index value, ranging between 108 and 161 (mean 138). Eight to twelve (commonly ten)
489 convolutions are visible in lateral view. Mean high of spiral cells is ~59 µm and they are
490 concave and ornamented with isolated small tubercles regularly arranged in row (Fig. 6I,
491 Q and T). Gyrogonites display a prominent psilocharoid-type apex (Fig. 6O and S). The
492 apex is ornamented with enlarged apical tubercles (Fig. 6S). The base is rounded or
493 slightly pointed showing a shallow pentagonal basal pore of ~36 µm in diameter (Fig. 6R
494 and U).

495 *Fossil record and distribution: Chara molassica* var. *notata* has been recovered in latest
496 Oligocene (Chattian) to Late Miocene (Tortonian) sedimentary sequences in Europe.
497 Feist-Castel (1977) and Feist and Ringeade (1977) described populations of this taxon
498 from the latest Oligocene/Early Miocene (Aquitanian) of the Provence and Aquitaine
499 basins in France respectively. Large samples of *C. molassica* var. *notata* were later
500 recovered in Aquitanian-aged rocks of the Alpine Molasse Basin in Switzerland (Berger
501 1983; Schwarz and Reichenbacher 1989). This variety is also well represented in the latest
502 Oligocene/Early Miocene of the Rhine Graben, Germany (Schwarz 1997 and references
503 therein). Julià de Agar (1991) reported this taxon from the Loranca Basin (Tagus Basin,
504 Spain). In the Ebro Basin (NE Spain) *C. molassica* var. *notata* is well represented in
505 Chattian to Tortonian non-marine deposits (Feist et al. 1994; González-Pardo 2012). This
506 species was also reported from the Middle East by Knobloch (1979) who found it in the
507 Miocene Fars Formation (Iraq).

508 *Palaeoecology:* Previous studies report this species in freshwater lacustrine facies (e.g.,
509 Feist and Ringeade 1977).

510

511 -----Figure 6 near here-----

512

513 *Chara* cf. *hispida* Linnæus, 1753

514 Fig. 7A–H

515 1753. *Chara hispida* Linnæus, p. 1156–1157

516 1989. *Chara hispida* var. *major* Soulié-Märsche, p. 92, pl. 23

517 1999. *Chara* cf. *hispida* var. *major* García, p. 311, Fig. 4a–e

518 *Material:* Hundreds of well-preserved gyrogonites have been recovered in the el Pi Gros
519 section (Table 1). One hundred specimens were measured from the sample PG2 (Table 2
520 in supplementary data).

521 *Description:* Gyrogonites are medium- to large-sized, ranging between 540–891 μm in
522 height (mean 726 μm) and 352–621 μm in width (mean 500 μm). The dominant
523 gyrogonite shape is prolate spheroidal to perprolate (Feist et al. 2005), with an isopolarity
524 index ranging between 106 and 206 (mean 145). Nine to twelve (commonly ten) spiral
525 cells are visible in lateral view (Fig. 7A–D). Spiral cells are flat to convex, about 88 μm
526 wide and without ornamentation. They become thinner towards the periphery of the apex.
527 The apex is psilocharoid and prominent, generally pointed (Fig. 7E–F). The base is also
528 pointed showing a small pentagonal basal pore of ~ 59 μm in diameter (Fig. 7G–H).

529 *Remarks:* The population at el Pi Gros displays smaller gyrogonites (~ 180 μm in length
530 and ~ 85 μm in width) than recent populations of *C. hispida* studied by Soulié-Marshé
531 (1989) or Détriché et al. (2009).

532 *Fossil record and distribution:* Fossils of *Chara hispida* have been described from
533 Quaternary sedimentary sequences of Europe, Africa and South America. Anadón et al.
534 (1987) reported gyrogonites of this species from the Pleistocene of the Guadix-Baza
535 Basin (SE Spain). Fossil samples are also reported from the Holocene lacustrine
536 sediments from the Wadi Shaw (Sudan) and intermountainous basins in the Middle Atlas
537 of Morocco (Soulié-Marsche 1991; Détriché et al. 2009). García (1999 and references
538 therein) reported gyrogonites of *C. hispida* from several Quaternary localities from
539 Argentina, i.e., Quebrada del Zonda (Province of San Juan), Laguna Salada Grande
540 (Buenos Aires Province), and Laguna del Bebedero (San Luis Province).

541 *Palaeoecology:* Extant *C. hispida* is a subcosmopolitan species thriving in lakes from
542 nearly all states in Europe, and a few localities in North Africa, the Caucasus, Central

543 Asia, and Eastern Siberia (Corillion 1972; Barinova et al. 2014 and references therein). It
544 dwells in alkaline permanent and well-oxygenated lakes at depths of up to 15 m.
545 However, this species mostly occurs between 0.5 and 7 m depth (Krause 1997). In spite
546 that preferred habitats of *C. hispida* are freshwater lakes, it can tolerate brackish water
547 (Mannscheck 2003). In agreement with habitat requirements of extant *C. hispida*, the
548 gyrogonite assemblage studied here would also be indicative of permanent and stable
549 freshwater lake conditions.

550 *Chara* sp.

551 Fig. 7I–M

552 *Material:* A few gyrogonites were found at el Pi Gros locality (Table 1). Three specimens
553 were measured in sample PG2 (Table 2 in supplementary data).

554 *Description:* Gyrogonites are very variable in size ranging between 612–825 μm in height
555 and 350–400 μm in width. The dominant gyrogonite shape is perprolate, with a very high
556 isopolarity index ranging between 161 and 206. Six to seven spiral cells are visible in
557 lateral view (Fig. 7J–L). Spiral cells are convex, without ornamentation. The apex is
558 psilocharoid and very prominent, generally pointed (Fig. 7I). The base is also pointed
559 showing a very small basal pore (Fig. 7M).

560 *Remarks:* This material could belong to extreme polymorphs of *Chara hispida*, with
561 which it cooccurs in the same samples but in a lower proportion (Table 1). Stressful
562 environmental conditions are well known to result in the development of extreme
563 polymorphs in extant *Chara* species (e.g., Pukacz et al. 2012).

564 Genus *Lamprothamnium* J. Groves, 1916

565 *Lamprothamnium papulosum* (Wallroth, 1833) comb. nov. Groves, 1916

566 Fig. 7N–U

567 1833. *Chara papulosa* Wallroth, p. 107

568 1916. *Lamprothamnium papulosum* Groves, p. 336

569 1969. *Lamprothamnium priscum* Castel and Grambast, p. 940–941, pl. XXXII, figs 4–7

570 1989. *Lamprothamnium papulosum* Soulié-Märsche, p. 150–153, pl. XXXII

571

572 *Material:* Many gyrogonites were recovered from several samples at the base of the
573 Vilobí del Penedès section (Table 1). Sixty specimens were measured from the sample
574 V5 (Table 2 in supplementary data).

575 *Description:* Gyrogonites are of medium size, 569–711 μm high (mean 631 μm) and 348–
576 542 μm wide (mean 469 μm), cylindrical or prolate in shape (Fig. 7N–Q), with an
577 isopolarity index ranging from 113 to 177 (mean 135). Gyrogonites show a prominent
578 apex of lamprothamnoid type (Fig. 7R–S), i.e., displaying a well-marked periapical
579 depression (Feist et al. 2005). Seven to eleven (commonly 9) spiral cells are visible in
580 lateral view. Spiral cells are concave, flat, or convex depending on the calcification degree
581 and ~ 81 μm high. Gyrogonites are not ornamented. The base of the gyrogonite is rounded
582 or slightly pointed with a small pentagonal pore, ranging in diameter from 40 to 60 μm
583 (Fig. 7T–U).

584 *Remarks:* Fossil gyrogonites of *L. papulosum* from Vilobí del Penedés are ~ 75 μm
585 wider and display a reduced number of spiral cells in lateral view than gyrogonites from
586 the living populations of the same species from brackish waters of southern France
587 studied by Soulié-Märsché (1989). The studied gyrogonites are morphologically closer to
588 *Lamprothamnium priscum* Castel and Grambast, 1969, a fossil species synonymized with
589 *L. papulosum* by Soulié-Märsche (1989).

590 *Fossil record and distribution:* Extant *Lamprothamnium papulosum* is a quasi-
591 cosmopolitan species distributed throughout the world except in North and Central
592 America (Corillion 1972; García and Chivas 2004). The oldest known *L. papulosum* was
593 reported by Castel and Grambast (1969) and referred to as *L. priscum*, from the early
594 Eocene deposits from the Corbières mountains (southern France) and further from the
595 early Eocene of Ksour Mountains in Algeria (Mennad et al. 2021). *Lamprothamnium*
596 *papulosum* has been found in several Quaternary deposits of North Africa (Soulié-
597 Märsche 1982, 1998, 2007).

598 *Palaeoecology:* *L. papulosum* is adapted to aquatic environments subject to salinity
599 fluctuations and can thrive in sub-saline to hyper-saline waters up to 68‰ in salinity
600 (Burne et al. 1980). Despite *Lamprothamnium* can live in hypersaline conditions, the
601 required salinity to produce oospores and gyrogonites should be 20–40‰ (Soulié-
602 Märsche 1998 and references therein). However, short periods of salinity close to 10‰
603 are also tolerated for germination of oospores and gyrogonites (Dubois, 1968).

604

605

606 -----Figure 7 near here-----

607

608 Genus *Lychnothamnus* (Ruprecht, 1845) von Leonhardi, 1863 emend. A. Braun in
609 Braun et Nordstedt, 1882

610 *Lychnothamnus barbatus* (Meyen, 1827) comb. nov. von Leonhardi, 1863

611 *Lychnothamnus barbatus* var. *antiquus* Soulié-Märsche, 1989

612 Fig. 8A–C

613 1827. *Chara barbata* Meyen, p. 75, pl. e, figs 7 and 8.

614 1863. *Lychnothamnus barbatus* Leonhardi, p. 72.

615 1989. *Lychnothamnus barbatus* var. *antiquus* Soulié-Märsche, p. 155, pl. 37, figs 1–6.

616 *Material:* A few specimens were recovered from the sample V6/7 at Vilobí del Penedès
617 (Table 1). Three gyrogonites were measured (Table 2 in supplementary data).

618 *Description:* Gyrogonites are large (878 μm high and 733 μm wide), ellipsoidal in shape
619 with an isopolarity index of 120. In the few gyrogonites recovered, spiral cells do not
620 display any modification in the width or thickness at the periphery of the apex (Fig. 8A).
621 The apex is flat, and the base is tapered showing a small basal pore. Nine or ten concave
622 spiral cells in lateral view separated by bicarinate sutures can be clearly observed near the
623 base (Fig. 8B). They are 120 μm high and devoid of ornamentation.

624 *Fossil record and distribution:* *Lychnothamnus barbatus* var. *antiquus* has been found in
625 several Miocene/Pliocene peri-Mediterranean lacustrine basins from Europe, North
626 Africa, and the Middle East. It has been reported from the Ebro and the Cerdanya basins
627 (NE Spain), Rio Maior (Portugal), Provence (France), Maoče (Montenegro), Çankırı
628 (Turkey) and Bekaa in Lebanon (Sanjuan and Alqudah 2018 and references therein).

629 *Palaeoecology:* The living species *L. barbatus* mainly thrives in permanent lakes of
630 northern Europe (Corillion 1972) where it forms dense meadows at depths ranging
631 between 2 and 8 m. These extant populations grow in cold and oligo-mesotrophic waters
632 of freshwater lakes, frequently associated to phreatic sources (Krause 1997; Brzozowski
633 et al. 2019).

634 *Lychnothamnus* sp.

635 Fig. 8D–F

636 *Material:* Only one complete specimen has been found. This gyrogonite and other
637 fragments attributed to this taxon were recovered from sample MA1 at Mas de l'Alonso
638 (Table 1 and Table 2 in supplementary data).

639 *Description:* Gyrogonites are large, 1022 μm high and 777 μm wide, cylindrical in shape
640 with an isopolarity index of 131. Spiral cells are ornamented with a characteristic
641 midcellular crest (Fig. 8E). Spiral cells do not show any modification at the periphery of
642 the apex and show a constant width. The apex is flat and ornamented with coma-shaped
643 tubercles (Fig. 8D). The base is tapered showing a star-shaped basal funnel (Fig. 8F).
644 Eight concave spiral cells are visible laterally, being separated by bicarinate sutures. This
645 character can be clearly observed near the base.

646 *Remarks:* The small number of recovered specimens hinders their identification to the
647 species level, but the ornamentation of this gyrogonite suggests affinities with species
648 formerly attributed to the fossil genus *Stephanochara* Grambast, which was synonymized
649 with *Lychnothamnus* by Soulié-Märsche (1989).

650 Genus *Nitellopsis* Hy, 1889

651 Subgenus *Tectochara* Grambast and Grambast-Fessard, 1954

652 *Nitellopsis (Tectochara) merianii* (Al. Braun ex Unger, 1852) comb. nov. Grambast and
653 Soulié-Märsche, 1972

654 Fig. 8G–N

655 1852. *Chara merianii* Unger, p. 82, pl. 25, figs 10–12.

656 1954. *Tectochara merianii* Grambast et Grambast-Fessard, p. 668.

657 1972. *Nitellopsis (Tectochara) merianii* Grambast et Soulié-Märsche, p. 11.

658 *Material:* Fifty gyrogonites were recovered from sample V6/7 at Vilobí del Penedès and
659 few fragments attributed to this taxon were found in sample MA1 (Table 1). Thirty-five
660 specimens were measured (Table 2 in supplementary data).

661 *Description:* Gyrogonites are large, ovoidal (Fig. 8K–N), 781–1120 µm high (mean 958
662 µm) and 656–957 µm wide (mean 824 µm), with an isopolarity index ranging between 104
663 and 135 (mean 116). Spiral cells are flat to convex. Seven to nine (frequently eight) spiral
664 cells are visible in lateral view (116 µm high). Gyrogonites display a nitellopsidoid apex
665 (Fig. 8G–H), i.e., spiral cells become thinner and narrower at the periapical zone (Horn
666 af Rantzien 1959). The apex is flat and ornamented with large apical nodules. The basal
667 pole is conical showing a basal pore within a wide pentagonal funnel, 292 µm in diameter
668 (Fig. 8I–J), sometimes star-shaped (Fig. 8J).

669 *Fossil record and distribution:* This species has been widely reported from several
670 Paleogene/Neogene basins from Europe, North Africa, the Middle East and Asia (Sanjuan
671 and Alqudah 2018 and references therein). The oldest representatives of this species were
672 discovered in latest Eocene (late Priabonian) deposits of the Ebro Basin (Sanjuan and
673 Martín-Closas 2014). Later, this species expanded its biogeographic range following 4
674 distributional phases to become finally subcosmopolitan in the Northern Hemisphere
675 during the Miocene (Soulié-Märsche et al. 1997; Soulié-Märsche et al. 2002; Sanjuan
676 and Martín-Closas 2015).

677 *Palaeoecology:* *Nitellopsis (T) merianii* is considered the ancestor of the living species
678 *Nitellopsis obtusa* (Sanjuan and Martín-Closas 2015). This taxon thrives in permanent,
679 cold, and deep alkaline lakes at a depth range between 4–12 m, in large lakes of northern
680 Europe, Asia and North America (Corillion 1972). This species cannot tolerate salinities
681 higher than 5‰ (Katsuhara and Tazawa 1986).

682 *Nitellopsis* sp.

Fig. 8O–Q

683

684 *Material:* A few abraded gyrogonites were recovered from sample V6/7, Vilobí del
685 Penedès. Only two specimens were measured (Table 2 in supplementary data).

686 *Description:* Gyrogonites are very large (1289 μm high and 1051 μm wide), ovoidal, with
687 an isopolarity index of 123. Spiral cells are flat and ornamented with a nodular mid-
688 cellular crest (Fig. 8P). Eight or nine spiral cells are visible in lateral view (155 μm high).
689 The apex is flat and of nitellopsidoid type (Horn af Rantzien 1959), ornamented with
690 small apical nodules (Fig. 8O). The basal pole is conical showing a small basal pore, 97
691 μm within a star-shaped funnel (Fig. 8Q).

692 *Remarks:* The main difference between this species and *N. (T) merianii* is the size and the
693 ornamentation. However, the small number of recovered specimens hinders their
694 identification to the species level.

695

696 -----Figure 8 near here-----

697

698 **Discussion**

699 *Charophyte taphonomy and palaeoecology*

700 The non-marine deposits from els Casots, Vilobí del Penedés, and Mas de l'Alonso–el Pi
701 Gros studied in this work have yielded a diverse number of charophyte and two ostracode
702 species which have characteristic palaeoenvironmental distributions. Several of them
703 have living representatives, which allow for more accurated palaeolimnological
704 inferences for the wetlands developed in the Vallès-Penedès and Vilanova i la Geltrú
705 basins during the Langhian and Serravalian.

706

707 We distinguish three different assemblages in the depositional environments studied:

708 *Charophytes from shallow lakes*: The microfossil assemblage associated to shallow lakes
709 varies locally. Charophyte assemblages at els Casots are dominated by *Chara* cf. *vulgaris*.
710 This living species has wide ecological tolerance and lives in brackish or freshwater
711 environments (estuaries, rivers, springs, ponds and lakes). It mostly occurs at very
712 shallow depths, from several centimeters up to 1 m and can live in eutrophic water
713 (Krause 1997). This species can withstand oligohaline conditions and it only produces
714 gyrogonites at salinities up to 5 ‰ (Ghetti et al. 2002). Associated taxa include *C.*
715 *molassica* var. *notata* and abraded tests of *Ammonia* sp. rotaliid foraminifera. *C.*
716 *molassica* var. *notata* is an extinct species related to freshwater lakes. The dominance of
717 *C. vulgaris* suggests very shallow water and that water trophism may have been high in
718 the paleolake of els Casots.

719 The flora in the upper part of the Vilobí del Penedès section (samples V5 and V6/7)
720 corresponds to a shallow lake as well. In this case the charophyte assemblage is dominated
721 by *C. molassica* var. *notata*. Other, less abundant, species include *Sphaerochara*
722 *ulmensis*, *Nitellopsis (Tectochara) merianii*, and *Lychnothamnus barbatus* var. *antiquus*.
723 A few poorly-preserved skeletons of rotaliid foraminifera (*Ammonia* sp.) also occur and
724 are considered allochthonous to the lake. Charophytes indicate the prevalence of
725 freshwater conditions. The occurrence of *Nitellopsis (Tectochara) merianii* and
726 *Lychnothamnus barbatus* var. *antiquus* (ancestors of the extant species *Nitellopsis obtusa*
727 and *Lychnothamnus barbatus*, respectively) thrive today in permanent, relatively deep
728 (2–8m), oligotrophic lakes with salinities not exceeding 5‰. The ecological requirements
729 of the charophyte assemblage at Vilobí del Penedès suggest that the lake was more stable
730 and oligotrophic than the contemporary lake of els Casots.

731 Finally, the assemblage from Mas de l'Alonso (sample MA1) also corresponds to shallow
732 lacustrine conditions. In spite of the scarce material recovered the charophyte assemblage
733 is quite diverse and also includes rare *Ammonia* sp. foraminifera. The charophyte
734 assemblage is constituted by *Sphaerochara ulmensis*, *Chara* cf. *hispida*, *Lychnothamnus*
735 sp. and fragmented gyrogonites attributed to *Nitellopsis (Tectochara) merianii*. This
736 assemblage indicates the prevalence of shallow freshwater conditions. *Ammonia* sp. tests
737 show evident signs of abrasion and are considered allochthonous, being probably
738 transported from nearby marine settings.

739 *Charophytes from coastal salinas*: Assemblages from Vilobí del Penedès (lower part of
740 the section) are dominated by the charophyte species *Lamprothamnium papulosum*,
741 which occurs associated to abraded ostracod carapaces. *L. papulosum* is the most
742 halotolerant species among living charophytes, surviving at salinities up to 70‰ (Burne
743 et al. 1980). Despite withstanding such hypersaline conditions, living populations of *L.*
744 *papulosum* require salinities around 20‰ (maximum 40‰) to produce gyrogonites
745 (Soulié-Märsche 1998 and references therein). The presence of monospecific
746 assemblages of *L. papulosum* at Vilobí del Penedès indicates the prevalence of brackish
747 water conditions, limiting the development of other charophyte species (Fig. 10). Several
748 germinated gyrogonites indicate that seasonally the palaeosalinity could have been going
749 down to 10‰ for short periods of time.

750

751 -----Figure 9 near here-----

752

753 *Charophytes from permanent lakes*: Based on the assemblages from el Pí Gros, two
754 charophyte species, *Chara* cf. *hispida* and *Chara* sp., and two ostracod taxa, *Heterocypris*

755 *salina* Brady 1868 (Fig. 9A–D) and a probable leptocytherid (Fig. 9E–J) are present. The
756 presence of articulated valves suggests *in situ* burial. Gyrogonites of *Chara* cf. *hispida*
757 are by far the dominant charophyte remains. Living meadows of *C. hispida* mainly grow
758 in alkaline permanent freshwater lakes at a depth up to 15 m, mainly between 0.5 and 7
759 m (Krause 1997). This is an eurythermal species preferring calcareous and well-
760 oxygenated waters (Barinova et al. 2014 and references therein), which can also tolerate
761 brackish water conditions, as reported from the Baltic Sea (Mannschreck 2003).. *Chara*
762 *hispida* shares similar habitat preferences with other *Chara* species and with *Nitellopsis*
763 *obtusata* (Barinova et al. 2014). While charophyte thalli are absent in the marls, charophyte
764 gyrogonites are very well preserved showing the endocalcine and ectocalcine layers
765 intact, without traces of corrosion or dissolution, thus evidencing that they were buried *in*
766 *situ* or near the production area. The ostracods found in these lacustrine facies provide
767 significant information about the characteristics of the palaeo-waterbody at el Pi Gros.
768 The leptocytherid species is similar to *Leptocythere* gr. *psammophila* in Gliozzi et al
769 (2005). *Heterocypris salina* Brady, 1868 is widely distributed across Europe, West Asia,
770 and North Africa inhabiting several types of waterbodies, from freshwater springs and
771 wells to littoral zones of seas (Meisch, 2000; Gusakov et al. 2021). This species is found
772 in slightly saline coastal and continental waters with salinities ranging from 5 to 35‰
773 (Gusakov et al. 2021), although Meisch (2000) reports that it is more usually associated
774 with oligosaline waters, with an optimum salinity preference of around 6 ‰. Meisch
775 (2000) further maintains that the species can also live in freshwater so that its presence
776 should not be regarded as indicative of a saline waterbody in the absence of supporting
777 evidence. Although Miocene leptocytherids have been reported from both marine
778 brackish and athalassic saline environments (Gliozzi et al. 2005), the co-occurrence of
779 the specimens with *H. salina*, together with additional micropalaeontological evidence,

780 suggests that el Pí Gros corresponds to lacustrine and oligohaline waterbody (Fig. 10).
781 This interpretation is consistent with the conclusions of Gliozzi et al (2005), who have
782 previously reported the co-occurrence of leptocytherids, including *Leptocythere* gr.
783 *psammophila* with *Heterocypris salina* from Serravallian lacustrine or palustrine
784 sediments from the Iberian Peninsula.

785

786 -----Figure 10 near here-----

787

788 **Conclusions**

789 Middle Miocene (Langhian–Serravallian) lacustrine deposits of the Vallès–Penedès and
790 Vilanova i la Geltrú basins (SW of Barcelona) are here analyzed from the
791 sedimentological and palaeoenvironmental viewpoints. The three localities studied, i.e.,
792 els Casots (Subirats), Vilobí del Penedès, and Mas de l’Alonso–el Pi Gros (Vilanova i la
793 Geltrú), yielded a well-preserved charophyte assemblage comprising ten different
794 species. The recovered flora shows a characteristic palaeoenvironmental distribution and
795 sheds new light on the prevailing palaeolimnological characteristics of the wetlands in
796 the coastal basins of NE Iberia during the Middle Miocene. Facies analysis, taphonomy
797 and palaeoecology of the recovered taxa allows for the distinction of three different
798 palaeoenvironmental settings: shallow lake, coastal salina, and permanent stable lake.
799 Claystones related to shallow lakes occur in the three studied localities and have yielded
800 *Sphaerochara ulmensis*, *Chara* cf. *vulgaris*, *Chara molassica* var. *notata*,
801 *Lychnothamnus barbatus* var. *antiquus*, *Lychnothamnus* sp., *Nitellopsis* (*Tectochara*)
802 *merianii*, and *Nitellopsis* sp. This flora is unevenly distributed owing to local
803 palaeolimnological conditions. Mesotrophic to eutrophic conditions dominated the

804 Langhian palaeolake at els Casots, while more oligotrophic and stable conditions might
805 have prevailed at the upper part of the Vilobí del Penedès (Langhian) section and at Mas
806 de l'Alonso (Serravallian). The occurrence of abraded tests of benthic foraminifera
807 suggests that these freshwater lakes were situated close to the coastline. Facies related to
808 coastal salinas are only found at the base of the Vilobí del Penedès section (Langhian)
809 and are characterized by primary gypsum beds alternated with greenish claystones rich in
810 *Lamprothamnium papulosum*. Monospecific populations of this halotolerant taxon
811 indicate the prevalence of brackish waters with salinity fluctuations from low to
812 hypersaline concentrations. However salinities of around 20‰ are needed for the
813 production of gyrogonites. Finally, charophytes found in marls and limestones attributed
814 to permanent stable lakes occurs at el Pi Gros (Serravallian). The lake was inhabited by
815 *Chara cf. hispida* and *Chara* sp. as well as the ostracod species *?Leptocythere* gr.
816 *psammophila* and *Heterocypris salina*, indicating the prevalence of oligohaline and well
817 oxygenated waters.

818 This is the first in-depth study of the charophytes from the Vallès-Penedès and Vilanova
819 basins. The results presented here show that charophytes are crucial for accurately
820 reconstructing palaeolimnological conditions, such as the water salinity, trophism or
821 depth. The combined study of charophytes and other microfossils, such as ostracods and
822 foraminifera, even improve such palaeoenvironmental inferences, especially regarding
823 salinity.

824 This study provides just a limited view of the total range of palaeoenvironments recorded
825 in this area. The whole Vallès sector and other associated sub-basins such as Sant Andreu
826 de la Barca, which contains mainly fluvio-lacustrine facies, have yet to be studied but
827 preliminary results indicate that they are also rich in charophyte fossils. Perhaps more
828 importantly, the combined continental record of these Catalan coastal basins covers

829 almost the entire Miocene, therefore allowing for the study of the evolution of terrestrial
830 wetland ecosystems along protracted time intervals.

831

832 **Acknowledgments**

833 This study was funded by the project IBERINSULA (PID2020-113912GB-100 / AEI /
834 10.13039/501100011033) of the Spanish Research Agency (AEI) and the European
835 Regional Development Fund (ERDF) and to project SGR2017-841 from the AGAUR
836 Research Agency (Catalan Autonomous Government). We thank Dr. Carles Ferràndez
837 (Department of Earth and Ocean Dynamics, Universitat de Barcelona) for his advice in
838 the determination of benthic foraminifera. Alejandro Gallardo (Laboratory of
839 Palaeontology, Department of Earth and Ocean Dynamics, Universitat de Barcelona) is
840 acknowledged for preparing the thin sections. We are also very thankful to David Artiaga
841 of the *Centres Científics i Tecnològics, Universitat de Barcelona* (CCiTUB) for his
842 technical support during the SEM sessions. Josep Rovira (Vilobí del Penedès) is
843 acknowledged for reporting us the charophyte beds from this locality. Dave Horne (Queen
844 Mary, University of London) advised on the ostracod identification. We also thank the
845 editor G. Dyke and the reviewer I. Soulié-Märsche for constructive comments during the
846 peer-review process.

847

848

849

850 **References**

- 851 Agardh CA. 1824. *Systema Algarum*. Lund, Lundae Literis Berlingianis, 312 p.
- 852 Agustí J, Cabrera L, Moyà-Solà S. 1985. Sinopsis estratigràfica del Neógeno de la fosa
853 del Vallès-Penedès. *Paleontologia i Evolució*. 18:57–81.
- 854 Agustí J, Cabrera L, Domènech R, Martinell J, Moyà-Solà S, Ortí F, de Porta J. 1990.
855 Neogene of the Penedès area (Prelittoral Catalan Depression, NE Spain).
856 *Paleontol Evol mem espec*. 2:187–207.
- 857 Agusti J, Cabrera L, Garces M, Pares JM. 1997. The Vallesian mammal succession in
858 the Vallès-Penedès Basin (northeast Spain): Paleomagnetic calibration and
859 correlation with global events. *Palaeogeogr. Palaeoclimatol. Palaeoecol*. 133 (3-
860 4): 149–180.
- 861 Alonso-Zarza AM, Wright VP. 2010. Palustrine carbonates. In: Alonso-Zarza AM,
862 Tanner LH, editors. *Carbonates in Continental Settings. Facies, Environments and*
863 *Processes: Developments in Sedimentology*, 61. Elsevier: Amsterdam, p. 103–
864 126.
- 865 Anadón P, Julià R, De Deckker P, Rosso JC, Soulié-Märsche I. 1987. Contribució de la
866 paleolimnologia del Pleistoceno inferior de la Cuenca de Baza (sector Orce-Vetna
867 Micena). *Paleontol Evol. mem. espec*. 1:35–72.
- 868 Baciu C, Feist M. 1999. Les charophytes Oligocènes du nord-ouest de la Transylvanie
869 (Roumanie). *Acta Palaeontol. Roman*. 2:27–29.
- 870 Barinova S, Romanov R, Solak CN. 2014. New record of *Chara hispida* (L.) Hartm.
871 (Streptophyta: Charophyceae, Charales) from the Işıklı Lake (Turkey) and Critical
872 Checklist of Turkish Charophytes. *Nat Resour Conserv*. 2 (3):33–42.

- 873 Bartrina MT, Cabrera L, Jurado MJ, Guimerà J, Roca E. 1992. Evolution of the central
874 Catalan margin of the Valencia trough (western Mediterranean). *Tectonophysics*.
875 203(1):219–247. [https://doi.org/10.1016/0040-1951\(92\)90225-U](https://doi.org/10.1016/0040-1951(92)90225-U)
- 876 Bathia SB, Soulié-Märsche I, Gemayel P. 1998. Late Pliocene and Early Pleistocene
877 charophyte floras of the Haripur Formation, Kerawa Group, Kashmir, India. *N.*
878 *Jb. Geol. Paläont. Abh.* 210 (2):185–209.
- 879 Batllori J, Moreno J. 2003. Nota preliminar sobre la malacofauna (Gastropoda) del Miocè
880 del Pi Gros (Vilanova i La Geltrú, Garraf): *Butll Inst Catalana Hist Nat.* 71:117–
881 127.
- 882 Belaústegui Z, Domènech R, Martinell J. 2018. An ichnofossil-lagerstätte from the
883 Miocene Vilanova Basin (Ne Spain): Taphonomic and paleoecologic insights
884 related to bioerosion structures. *Palaios* 33:16–28.
- 885 Bessedik M. 1985. Reconstitution des environnements miocènes des régions nord-ouest
886 méditerranéennes à partir de la palynologie. PhD Thesis, Université des Sciences
887 et Techniques du Languedoc, Montpellier: 162 p.
- 888 Berger JP. 1983. Charophytes de l’Aquitanién de Suisse occidentale. Essai de taxonomie
889 et biostratigraphie. *Geobios* 16 (1):5–37.
- 890 Bitzer K. 2004. Estimating paleogeographic, hydrological and climatic conditions in the
891 upper Burdigalian Vallès–Penedès Basin (Catalunya, Spain). *Geol. Acta* 2:321–
892 31.
- 893 Brady G. 1868. A monograph of the recent British Ostracoda. *Transactions of the Linnean*
894 *Society of London* 26:353–495.

- 895 Braun A, Nordstedt O. 1882. Fragmente einer Monographie der Characeen nach den
896 hinterlassenen Manuskripte A. Braun's, herausgegeben von Dr. O. Nordstedt.
897 Berlin, Abhandlungen der Kaiserlichen Akademie der Wissenschaften, p. 211.
- 898 Brzozowski M, Palomares-Cabanilles M, Kowalewski G, Pełechaty M. 2019.
899 Environmental factors responsible for the gyrogonite formation by an endangered
900 macroalga, *Lychnothamnus barbatus*, a fertility indicator of past and present
901 lacustrine ecosystems. *Limnologica* 77:125686.
- 902 Burne RV, Bauld JI, Deccker P. 1980. Saline lake charophytes and their geological
903 significance. *J. Sediment. Petrol.* 50:281–293.
- 904 Cabrera L. 1979. Estudio estratigráfico y sedimentológico de los depósitos continentales
905 basales de la depresión del Vallès-Penedès [dissertation]. Barcelona: Universitat
906 de Barcelona.
- 907 Cabrera L. 1981a. Influencia de la tectónica en la sedimentación continental de la
908 cuenca del Vallès-Penedès (provincia de Barcelona, España) durante el Mioceno
909 inferior. *Acta Geol Hisp.* 16:163–169.
- 910 Cabrera L. 1981b. Estratigrafía y características sedimentológicas generales de las
911 formaciones continentales del Mioceno inferior de la cuenca del Vallés Penedés
912 (Barcelona, España). *Estud Geol.* 37:35–44.
- 913 Cabrera L, Calvet F. 1996. The onshore Neogene record in NE Spain: Vallès-Penedès
914 and El Camp half-grabens (NW Mediterranean). In: Friend PF, Dabrio CJ,
915 editors. *Tertiary Basins of Spain: Record of Crustal Kinematics*. Cambridge,
916 United Kingdom: Cambridge University Press; p. 97–105.
- 917 Cabrera L, Calvet F, Guimerà J, Permanyer A. 1991. El registro sedimentario miocénico
918 en los semigrabens del Vallès–Penedès y de El Camp: organización secuencial y

919 relaciones tectónica-sedimentación. In: Colombo, F, editor. Libro Guía nº 4 del
920 Congreso del GET, Vic: 132 p.

921 Cabrera L, Roca E, Garcés M, de Porta J. 2004. Estratigrafía y evolución
922 tectonosedimentaria Oligocena superior-Neógena del sector central del margen
923 Catalán (Cadena Costero-Catalana). In: Vera JA. editor. Geología de España,
924 Sociedad Geológica de España, Instituto Geológico y Minero de España: 569–
925 573.

926 Casanovas-Vilar I, DeMiguel D, Galindo J, Robles JM, Garcés M, Cabrera L. 2011. The
927 continental Burdigalian (Early Miocene) of the Vallès–Penedès Basin (Catalonia,
928 Spain). In: Pérez-García A, Gascó F, Gasulla JM, Escaso F. editors. Viajando a
929 Mundos Pretéritos. Ayuntamiento de Morella, Morella: p. 93–100.

930 Casanovas-Vilar I, Madern A, Alba DM, Cabrera L, García-Paredes I, Van den Hoek
931 Ostende LW, De Miguel D, Robles JM, Furió M, Van Dam J, Garcés M, Angelone
932 C, Moyà-Solà S. 2016a. The Miocene mammal record of the Vallès–Penedès
933 Basin (Catalonia). *C R Palevol*. 15:791–812.

934 Casanovas-Vilar I, Garcés M, Van Dam J, García-Paredes I, Robles JM, Alba DM. 2016b.
935 An updated biostratigraphy for the late Aragonian and the Vallesian of the Vallès-
936 Penedès Basin (Catalonia). *Geol Acta* 14 (3):195–217.

937 Casanovas-Vilar I, Garcés M, Marcuello A, Abella J, Madurell-Malapeira J, Jovells-
938 Vaqué S, Cabrera LI, Galindo J, Beamud E, Ledo JJ, Queralt P, Martí A, Sanjuan
939 J, Martín-Closas C, Jiménez-Moreno G, Luján AH, Villa A, DeMiguel D, Sanchez
940 I, Robles JM, Furió M, Van den Hoek Ostende LW, Sanchez-Marco A, Sanisidro
941 O, Valenciano A, Garcia-Paredes I, Angelone C, Pons-Monjo G, Azanza B,
942 Delfinor M, Bolet A, Grau-Camats M, Vizcaíno-Varo V, Mormeneo D, Kimura

943 Y, Moyà-Solà S, Alba DM. 2022. Els Casots (Subirats, Catalonia), a key site for
944 the Miocene vertebrate record of Southwestern Europe. *Hist Biol.* 34 (8):1494–
945 1508.

946 Castel M, Grambast L. 1969. Charophytes de l'Éocène des Corbières. *Bull Soc Géol Fr.*
947 7 (11):936–943.

948 Chellaï EH, Baudelot S, Crochet B, Feist M, Durand-Delga M. 1982. Preuves
949 paléontologiques de l'antériorité des Conglomérats de la Grésine (Éocène
950 supérieur) par rapport à la Molasse oligocène de l'Albigeois (Tarn). *C. R. Acad.*
951 *Sci. Paris* 295:683–690.

952 Corillion R. 1972. Les Charophycées de France et d'Europe Occidentale. *Travaux du*
953 *Laboratoire de Botanique de la Faculté des Sciences d'Angers, Angers:* 11–12,
954 499 p.

955 de Gibert JM, Casanovas-Vilar I. 2011. Contexto geológico del Mioceno de la cuenca del
956 Vallès-Penedès. *Paleontologia i Evolució. Mem. espec.* 6: 39–45.

957 Détriché S, Bréhéret JG, Soulié-Märsche I, Karrat L, Macaire JJ. 2009. Late Holocene
958 water level fluctuations of Lake Afourgagh (Middle-Atlas Mountains, Morocco)
959 inferred from charophyte remains. *Palaeogeogr Palaeoclimatol Palaeoecol.*
960 283:134–147.

961 Dubois, A. 1968. Observations sur la morphologie et la biologie des formes naines de
962 *Lamprothamnium papulosum* J. Groves (Characées). *Naturalia Monspeliensia Ser*
963 *Bot.* 19:37–41.

964 Fan H, Gasse F, Huc A, Li Y, Sifeddine A, Soulié-Märsche I. 1996. Holocene
965 environmental changes in Bangong Co basin (Western Tibet). Part 3: Biogenic
966 remains. *Palaeogeogr Palaeoclimatol Palaeoecol.* 120:65–78.

- 967 Feist-Castel M. 1977. Etude floristique et biostratigraphique des Charophytes dans les
968 series du Paleogene de Provence. Géol. Médit. 4:109–138.
- 969 Feist M, Ringeade M. 1977. Étude biostratigraphique et paléobotanique (charophytes)
970 des formations continentales d'Aquitaine, de l'Éocène supérieur au Miocène
971 inférieur. Bull Soc Géol Fr. 7:341–354.
- 972 Feist M, Anadón P, Cabrera L, Choi SJ, Colombo F, Saez M. 1994. Upper Eocene-
973 Lowermost Miocene charophyte in the Ebro Basin (Spain). Contribution to the
974 charophyte biozonation in Western Europe. Newsl Stratigr. 30:1–32.
- 975 Feist M, Grambast-Fessard N, Guerlesquin M, Karol K, Lu H, Mccourt RM, Wang Q,
976 Shenzen Z. 2005. Treatise on Invertebrate Paleontology. Part B., Protoctista 1.
977 Charophyta, The Geological Society of America, Kansas: 170 p.
- 978 Fontboté JM. 1954. Las relaciones tectónicas de la depresión del Vallès–Penedès con la
979 Cordillera Prelitoral Catalana y con la Depresión del Ebro. In: CSIC editor. Tomo
980 extraordinario de trabajos geológicos publicado con motivo del 80 aniversario del
981 nacimiento del profesor Eduardo Hernández-Pacheco. R Soc Esp Hist Nat. p. 281–
982 310.
- 983 Foster GL, Lear CH, Rae JWB. 2012. The evolution of pCO₂, ice volume and climate
984 during the middle Miocene. Earth Planet Sci Lett. 341–344:243–254.
985 <https://doi.org/10.1016/j.epsl.2012.06.007>
- 986 García A. 1999. Quaternary charophytes from Salina del Bebedero, Argentina: Their
987 relation with extant taxa and palaeolimnological significance. J Paleolimnol.
988 21:307–323.
- 989 García A, Chivas AR. 2004. Quaternary and extant euryhaline *Lamprothamnium* Groves
990 (Charales) from Australia: Gyrogonite morphology and paleolimnological

- 991 significance. *J Paleolimnol.* 31(3):321–341. Ghetti P, Anadón P, Bertini A, Esu D,
992 Gliozzi E, Rook L, Soulié-Märsche I. 2002. The Early Messinian Velona Basin
993 (Siena, Central Italy): Paleoenvironmental and paleobiogeographical
994 reconstructions. *Palaeogeogr Palaeoclimatol Palaeoecol.* 187:1–33.
- 995 Gierlowski-Kordesch EH. 2010. Lacustrine carbonates. In: Alonso-Zarza AM, Tanner
996 LH, editors. *Carbonates in Continental Settings. Facies, Environments and*
997 *Processes: Developments in Sedimentology*, 61. Elsevier, Amsterdam: p. 1–101.
- 998 Gliozzi E, Rodriguez-Lazaro J, Nachite D, Martin-Rubio M, Bekkali R. 2005. An
999 overview of Neogene brackish leptocytherids from Italy and Spain:
1000 Biochronological and palaeogeographical implications. *Palaeogeogr*
1001 *Palaeoclimatol Palaeoecol.* 225:283–301.
- 1002 González-Pardos M. 2012. Carófitos del Mioceno inferior de la Formación Tudela
1003 (Cuenca del Ebro, Navarra). Master's thesis, Universitat de Valencia: 69 p.
- 1004 Grambast L. 1962. Aperçu sur les Charophytes tertiaires du Languedoc et leur
1005 signification stratigraphique. *C R Somm Séances Soc Géol Fr.* 10:313–314.
- 1006 Grambast L, Grambast-Fessard N. 1954. Sur la position systématique de quelques
1007 charophytes tertiaires. *Rev Gén Bot.* 61:665–771.
- 1008 Grambast L, Paul P. 1965. Observations nouvelles sur la flore de charophytes du
1009 Stampien du bassin de Paris. *Bull Soc Géol Fr.* 7:239–247.
- 1010 Grambast L, Soulié-Märsche I. 1972. Sur l'ancienneté et la diversification des *Nitellopsis*
1011 (Charophytes). *Paléobiol cont.* 3:1–14.
- 1012 Groves J. 1916. On the name *Lamprothamnus* Braun. *J Bot.* 54:336–337.

- 1013 Guimerà J. 1992. Les fosses i depressions Neògenes. Història natural dels Països
1014 Catalans. Geologia 2. Enciclopedia Catalana, S.A. Barcelona: 548 p.
- 1015 Gusakov VA, Makhutova ON, Gladyshev MI. Golovatyuk LV, Zinchenko TD. 2021.
1016 Ecological role of *Cyprideis torosa* and *Heterocypris salina* (Crustacea,
1017 Ostracoda) in saline rivers of the Lake Elton basin: abundance, biomass,
1018 production, fatty acids. Zool Stud. 60:60–53.
- 1019 Holbourn A, Kuhnt W, Kochhann KGD, Andersen N, Sebastian Meier KJ. 2015. Global
1020 perturbation of the carbon cycle at the onset of the Miocene Climatic Optimum.
1021 Geology. 43(2):123–126. <https://doi.org/10.1130/G36317.1>
- 1022 Horn af Rantzien H. 1959. Morphological types and organ-genera of Tertiary Charophyte
1023 fructifications. Stockh Contrib Geol. 4:45–197.
- 1024 Huang RJ, Zhong ZQ, Nie YS. 1988. Early Tertiary Charophytes from the Dongpu
1025 region. In: Series on Stratigraphy and Paleontology of Oil and Gas bearing Areas
1026 in China. Research Institute of Exploration and Development, Zhongyuan
1027 Petroleum Exploration Bureau and Nanjing Institute of Geology and
1028 Paleontology, The Petroleum Industry Press, Beijing: 188 p.
- 1029 ICC (Institut Cartogràfic de Catalunya). [ICGC - Vissir3 \(icc.cat\)](http://www.icc.cat) (accessed 15 April
1030 2021). Janis CM. 1993. Tertiary mammal evolution in the context of changing
1031 climates, vegetation, and tectonic events. Annu Rev Ecol Syst. 24:467–500.
- 1032 Jovells-Vaqué S. 2020. Early Miocene cricetids from the Vallès- Penedès Basin
1033 (Catalonia): taxonomy, biostratigraphy and paleoecological implications. PhD
1034 Thesis, Universitat Autònoma de Barcelona, Bellaterra: 370 p.
- 1035 Jovells-Vaqué S, Casanovas-Vilar I. 2021. Dispersal and early evolution of the first
1036 modern cricetid rodents in Western Europe: new data from the Vallès-Penedès

- 1037 Basin (Catalonia). *Comptes Rendus Palevol.* 20(22):401–439.
- 1038 <https://doi.org/10.5852/cr-palevol2021v20a22>
- 1039 Julià de Agar JJ. 1991. Contribución al estudio de carófitos fósiles de la Cuenca Terciaria
1040 de Loranca (provincia de Cuenca, España). *Coloquios de Paleontología* 43:57–78.
- 1041 Katsuhara M, Tazawa M. 1986. Salt tolerance in *Nitellopsis obtusa*. *Protoplasma*
1042 135:155–161.
- 1043 Knobloch E. 1979. Fossil Charophyta from the Neogene and Holocene of Iraq. *Věst Ústř*
1044 *Úst Geol.* 54: 237–241.
- 1045 Korsch H. 2016. *Chara vulgaris*, In: Arbeitsgruppe Characeen Deutschlands, editors.
1046 Armeleucheralgen. *Die Characeen Deutschlands*. Springer Verlag, Heidelberg: p.
1047 379–387.
- 1048 Krause W. 1997. Charales (Charophyceae). *Süßwasserflora von Mitteleuropa*. Band 18.
1049 Gustav Fischer Verlag, Jena: 202 p.
- 1050 Leonhardi H Von. 1863. Über die böhmischen Characeen. *Lothos* 13:55–62.
- 1051 Lindley J. 1836. *A Natural System of Botany*. Longman, 2nd edition, London: 526 p.
- 1052 Linnæus C. 1753. *Species plantarum, exhibentes plantas rite cognitatas, ad genera relatas,*
1053 *cum differentiis specificis, nominibus trivialibus, synonymis selectis, loci*
1054 *natalibus, secundum sexuale digestas, vol. 2.* Impensis Laurentii Salvii.
1055 Stockholm: p. 561–1.200.
- 1056 Liu JY. 1989. Cenozoic Paleobiota of the continental shelf of the East China Sea
1057 (Donghai). Geological Publishing House, Beijing: 324 p.
- 1058 Lu H, Luo Q. 1990. Fossil Charophytes from the Tarim Basin. Xinjiang. Series on
1059 Stratigraphy and Palaeontology of oil and gas bearing areas in China. Science and
1060 Technical Documents Publishing House, Beijing: 261 p.

- 1061 Ludwig K. 1987. Mikropaläontologische Hinweise für die autochthone Entstehung der
1062 miozänen Braunkohle im Becken von Teruel-Ademuz (NE- Spanien) Paläontol Z.
1063 61:17–27.
- 1064 Mädler K. 1952. Zur Taxonomie der Tertiären Charophyten. Geol Jahrb. 70:265–328.
- 1065 Mädler K. 1955. Charophyten aus dem Nordwestdeutschen Kimmeridge. Geol Jahrb. 67,
1066 1–46.
- 1067 Mädler K, Staesche U. 1979. Fossile Charophyten aus dem Känozoikum (Tertiär und
1068 Quartär) der Türkei. Geol Jahrb. B 33:81–157.
- 1069 Mannschreck B. 2003. *Chara hispida* (L.) Hartm. 1820. In: Schubert I, Blindow H,
1070 editors. Charophytes of the Baltic Sea. Gantner Verlag, Ruggell, Liechtenstein: p.
1071 107–112.
- 1072 Martín-Closas C. 1999. Epiphytic overgrowth of charophyte thalli by stromatolite-like
1073 structures and fungi in the Lower Cretaceous of the Iberian Ranges (Spain). Aust
1074 J Bot. 47: 305–313.
- 1075 Martín-Closas C, Ramos E. 2005. Palaeogene Charophytes of the Balearic Islands
1076 (Spain). Geol Acta. 3:39–58.
- 1077 Meisch C. 2000. Freshwater Ostracoda of Western and Central Europe. Süßwasserfauna
1078 von Mitteleuropa 8/3. Gustav Fischer, Stuttgart, 522 p.
- 1079 Meyen F. 1827. Beobachtung und Bemerkungen über die Gattung *Chara*. Linnaea
1080 2(1):55–81.
- 1081 Mennad A, Adaci M, Tabuce R, Martín-Closas C, Benyoucef M, Bensalah M, Otero O,
1082 Sarr R, Zaoui D. 2021. Découverte de charophytes et ostracodes de l'Yprésien
1083 inférieur dans les Monts des Ksour (Algérie): biostratigraphie et paléoécologie.
1084 Ann Paléontol. 107:102466.

- 1085 Migula W. 1897. Die Characeen, In: Rabenhorst L, editor. Kryptogamen-Flora von
1086 Deutschland, Oesterreich und der Schweiz. E. Kummer, Leipzig: 772 p.
- 1087 Miller KG, Browning JV, Schmelz WJ, Kopp RE, Mountain GS, Wright JD. 2020.
1088 Cenozoic sea-level and cryospheric evolution from deep-sea geochemical and
1089 continental margin records. Science Advances. 6(20): eaaz1346.
1090 <https://doi.org/10.1126/sciadv.aaz1346>
- 1091 Ortí F. 1990. Yesos de Vilobí (Mioceno). In: Ortí F, Salvany JM, editors. Formaciones
1092 evaporíticas de la Cuenca del Ebro y cadenas periféricas, y de la zona de Levante
1093 Barcelona, ENRESA: 306 p.
- 1094 Ortí F, Pueyo JJ. 1976. Yeso primario y secundario de depósito de Vilobí (provincia de
1095 Barcelona, España). Publicaciones del Instituto de Investigaciones Geológicas,
1096 Universidad de Barcelona 31:5–34.
- 1097 Ortíz JE, García-Cortés E, Colliga LA, Mansilla H, Torres T. 1998. Yacimientos de
1098 carofitas en la Depresión Intermedia (Cuenca, Guadalajara, España central).
1099 Geogaceta 23:115–118.
- 1100 Permanyer A. 1990. Sedimentologia i diagènesi dels esculls miocènics del Penedès.
1101 Arxius de les Seccions de Ciències, Institut d'Estudis Catalans 92: 321 p.
- 1102 Pukacz A, Boszke P, Pelechaty MJ, Raabe U. 2012. Comparative study of the oospore
1103 morphology of two populations of a rare species *Chara baueri* A. Braun in
1104 Cedynia (Poland) and Batzlow (Germany). Acta Soc Bot Pol. 81:131–136.
- 1105 Ramos-Guerrero E, Casas A, Pinto V, Agustí J. 1996. Estructura y relleno sedimentario
1106 de la semifosa Neógena de Vilanova (Garraf, Barcelona). Acta Geol Hisp. 29:93–
1107 106.

- 1108 Rasky K. 1945. Fossile Charophyten-Früchte aus Ungarn. Ungarischen
1109 Naturwissenschaftlichen Museums 2:1–75, 3 pl.
- 1110 Reichenbacher B, Schwarz J. 1997. Charophyten und Otolithen aus den Cyrenen-
1111 Schichten des nördlichen Alpenvorlandes. PalZ. 71:173–188.
- 1112 Roca E. 2001. The northwest Mediterranean (Valencia through, Gulf of Lyons and
1113 Liguro-Provençal basins): structure and geodynamic evolution. In: Ziegler PA,
1114 Cavazza W, Robertson AHF, Crasquin-Soleau S, editors. Peritehtyan rift/wrench
1115 basins and passive margins. Mém Mus Hist Natl Paris 186:671–706.
- 1116 Roca E, Guimerà J. 1992. The Neogene structure of the eastern Iberian margin: structural
1117 constraints on the crustal evolution of the Valencia through (Western
1118 Mediterranean). Tectonophysics 203:203–218.
- 1119 Roca E, Sans M, Cabrera L, Marzo M. 1999. Oligocene to Middle Miocene evolution of
1120 the Central Catalan margin (North-western Mediterranean). Tectonophysics 315:
1121 209–229.
- 1122 Ruprecht FJ. 1845. Distributio Cryptogamarum Vascularium in Imperio Rossico.
1123 Beiträge der Pflanzenkunde des Russischen Reiches 3: 56 p.
- 1124 Sanjuan J, Alqudah M. 2018. Charophyte flora from Miocene deposits of Zahle (Beeka
1125 Valley, Lebanon). Biostratigraphic, Palaeoenvironmental and
1126 Palaeobiogeographical implications. Geodiversitas 40 (10):195–209.
- 1127 Sanjuan J, Martín-Closas C. 2014. Taxonomy and palaeobiogeography of charophytes
1128 from the Upper Eocene-Lower Oligocene of the eastern Ebro basin (Catalonia,
1129 NE Spain). Geodiversitas 36 (3):385–420.
- 1130 Sanjuan J, Martín-Closas C. 2015. Biogeographic history of two Eurasian Cenozoic
1131 charophyte lineages. Aquat Bot. 120 (A):18–31.

- 1132 Sanjuan J, Vicente A, Flor-Arnau N, Monleón T, Cambra J, Martín-Closas C. 2017.
1133 Effects of light and temperature on *Chara vulgaris* gyrogonite productivity and
1134 polymorphism. Paleoenvironmental implications. *Phycologia* 56 (2):204–212.
- 1135 Sanz de Siria Catalán A. 1993. Datos sobre la paleoclimatología y paleoecología del
1136 Neógeno del Vallès-Penedès según las macrofloras halladas en la cuenca y zonas
1137 próximas. *Paleontologia i Evolució* 26–27:281–289.
- 1138 Sanz de Siria Catalán A. 1994. La evolución de las paleofloras en las cuencas cenozoicas
1139 catalanas. *Acta Geol Hisp.* 29:169–189.
- 1140 Schwarz J. 1997. Charophyten aus dem Tertiär des Oberrheingrabens (Mitteleozän-
1141 Untermiozän). *Palaeontographica B* 243:1–84.
- 1142 Schwarz J. Reichenbacher B. 1989. Die Charophytenflora der Kirchberger Schichten
1143 (Unter-Miozän). *Geol Bavarica.* 94:179–193.
- 1144 Smith GM. 1938. Botany. Algae and Fungi. Charophyceae. New York, McGraw Hill, 1:
1145 127 p.
- 1146 Soulié-Märsche I. 1978. Contributions a la Paléontologie du Miocène Moyen continental
1147 du Bassin du Tage. IV-Charophytes-Póvoa de Santarém, Pêro Filho et Tremês.
1148 Ciências da Terra. *Earth Sciences Journal* 4:91–102.
- 1149 Soulié-Märsche I. 1982. Lac pléistocène du Fezzan (Libye). In: Le Shati (editions du
1150 centre national de la recherche scientifique). Marseille, France: p. 80–85.
- 1151 Soulié-Märsche I. 1989. Étude comparée de gyrogonites de charophytes actuelles et
1152 fossiles et phylogénie des genres actuels. Millau, Imprimerie des Tilleuls: 237 p.
- 1153 Soulié-Märsche I. 1991. Charophytes as lacustrine biomarkers during the Quaternary in
1154 North Africa. *J Afr Earth Sci.* 12 (1/2):341–351.

- 1155 Soulié-Märsche I. 1998. Fossil *Lamprothamnium papulosum* (Charophyta), a biomarker
1156 for seasonal rainfall in northern Mauritania. In: Heine K, editor. Paleoecology of
1157 Africa 25: p. 65–76.
- 1158 Soulié-Märsche I. 2007. Charophytes, indicators for low salinity phases in North sebkhet.
1159 J Afr Earth Sci. 51:69–76.
- 1160 Soulié-Märsche I. Martín-Closas, C. 2003. *Lychnothamnus barbatus* (Charophytes) from
1161 the Upper Miocene of La Cerdanya (Catalonia, Spain): taxonomic and
1162 palaeoecological implications. Acta Micropal Sinica. 20:156–165.
- 1163 Soulié-Märsche I, Gemayel P, Chaimanee Y, Suteethorn V, Jaeger JJ, Ducrocq S. 1997.
1164 *Nitellopsis* (Charophyta) from the Miocene of northern Thailand. Alcheringa
1165 21:141–156.
- 1166 Soulié-Märsche I, Benammi M, Gemayel P. 2002. Biogeography of living and fossil
1167 *Nitellopsis* (Charophyta) in relationship to new finds from Morocco. J Biogeogr.
1168 29:1703–1711.
- 1169 Soulié-Märsche I, Bieda S, Lafond R, Maley J, Baitoudji M, Vincent PM, Faure H. 2010.
1170 Charophytes as bio-indicators for lake level high stand at “Trou au Natron”,
1171 Tibesti, Chad, during the Late Pleistocene. Glob Planet Change. 72 (4):334–340.
- 1172 Steinthorsdottir M, Coxall HK, Boer AM de, Huber M, Barbolini N, Bradshaw CD, Burls
1173 NJ, Feakins SJ, Gasson E, Henderiks J, Holbourn AE, Kiel S, Kohn J, Kürschner
1174 VM, Lear CH, Liebrand D, Kunt DJ, Mörs T, Pearson PN, Pound MJ, Stoll H,
1175 Strömberg E. 2020. The Miocene: the future of the past. Paleocanogr
1176 Paleoclimatol. 36(4): e2020PA004037. <https://doi.org/10.1029/2020PA004037>.
- 1177 Straub EW. 1952. Mikropaläontologische Untersuchungen im Tertiär zwischen Ehingen
1178 und Ulm an der Donau. Geol Jahrb. 66:433–524.

- 1179 Tang L, Di H. 1991. Fossil charophytes from Qaidam basin, Qinghai. Beijing: 220 p., 79
1180 pl. (in Chinese with abstract and table in English).
- 1181 Unger F. 1852. *Iconographia plantarum fossilium*. Denkschriften Akademie der
1182 Wissenschaften, Mathematisch-Naturwissenschaftliche Klasse, Wien 4: p. 73–118.
- 1183 Van Dam JA, Krijgsman W, Abels HA, García-Paredes I, López Guerrero P, Peláez-
1184 Campomanes P, Ventura D. 2014. Updated chronology for Middle to Late Miocene
1185 mammal sites of the Daroca area (Calatayud-Montalbán Basin, Spain). *Geobios*.
1186 47:325–334.
- 1187 Van der Meulen AJ, García-Paredes I, Álvarez Sierra MÁ, Van den Hoek Ostende LW,
1188 Hordijk K, Oliver A, Pélaez-Campomanes P. 2012. Updated Aragonian
1189 biostratigraphy: small mammal distribution and its implications for the Miocene
1190 European chronology. *Geol Acta*. 10:159–179.
1191 <https://doi.org/10.1344/105.000001710>
- 1192 Wallroth FG. 1833. *Flora cryptogamia Germaniae. Pars posterior. Continens Algas et*
1193 *Fungos*. In: Bluff MJ, Fingerhuth CA, editors. *Compendium florae Germanicae*.
1194 *Sectio II plantae cryptogamicae sine cellulosa*. Tomus IV: 923 p.
- 1195 Xinlun Z. 1978. Early Tertiary Charophytes from Coastal Region of Bohai. Nanjing
1196 Institute of Geology and Paleontology. Nanjing (in Chinese): 49 p.
- 1197 You Y, Huber M, Müller RD, Poulsen CJ, Ribbe J. 2009. Simulation of the Middle
1198 Miocene Climate Optimum. *Geophys Res Lett*. 36:L04702.
1199 [doi:10.1029/2008GL036571](https://doi.org/10.1029/2008GL036571).
- 1200 Zachos J, Pagani M, Sloan L, Thomas E, Billups K. 2001. Trends, rhythms, and
1201 aberrations in global climate 65 Ma to present. *Science*. 292(5517):686–693.
1202 <https://doi.org/10.1126/science.1059412>.

1203 Zachos JC, Dickens GR, Zeebe RE. 2008. An early Cenozoic perspective on greenhouse
1204 warming and carbon-cycle dynamics. *Nature*. 451(7176):279–283.
1205 <https://doi.org/10.1038/nature06588>.

1206

1207 **Figure captions**

1208 Figure 1. Geological map of the study area. Red stars represent the location of the three
1209 studied localities in the Vallès-Penedès and Vilanova i la Geltrú basins. V=Vilobí;
1210 E.C=els Casots; M.A= Mas de l'Alonso; P.G=el Pí Gros. Modified from ICC (2021).

1211 Figure 2. Stratigraphic logs of the 4 studied localities. 1) els Casots (Subirats); 2) Vilobí
1212 del Penedès; 3) el Pí Gros (Vilanova i la Geltrú); 4) Mas de l'Alonso (Vilanova i la
1213 Geltrú).

1214 Figure 3. Facies and microfacies from els Casots (Subirats). A–B. Field photos of the
1215 stratigraphic section. A. organic-claystones with pedogenetic features, see the location of
1216 the sample C4. B. limestone interval from where the samples C2 was extracted. C–H.
1217 Microphotographs of the limestone sample C2. C. Packstone of cyanobacterial crusts. D.
1218 subrounded oncoïd. E. fragments of mollusk shells (m.s). F. detail of a mollusk shell. G.
1219 well-developed oncoïd (Onc). H. detail of cyanobacterial crusts.

1220 Figure 4. Field photos of the section at Vilobí del Penedès. A. laminated gypsarenite
1221 interval at the base of the section. B. gypsum (G) and claystone alternation at the base of
1222 the section, see the position of samples yielding charophytes V1, V3, and V4. C. Partially
1223 covered greenish claystones, see the position of the sample V5. D. Oyster bank at the top
1224 of the section.

1225 Figure 5. Facies and microfacies from the el Pi Gros locality (Vilanova i la Geltrú). A.–
1226 B. Field photos of the stratigraphic section. A. general overview of the upper half section.
1227 B. facies showing a shallowing upward cycle from base to top; marly limestone (M),
1228 wackestone-packstone limestone (W-P. L), stromatolitic limestone (S.L) and bioturbated
1229 claystone (B.C). C–F. Microphotographs of the sample PG1. C. wackstone with
1230 gyrogonites (Gyr). D. Detail of a *Chara* gyrogonite showing the basal plate (B.P). E.
1231 wackestone–packstone with ostracods (ostr). F. wackestone–packstone with charophytes

1232 showing diagenetic dissolution. G–H. Microphotographs of PG4 sample, wackestone–
1233 packstone with ostracods (ostr), gyrogonites (gyr), and thalli.

1234 Figure 6. Fossil charophytes from the Vallès-Penedès and Vilanova i la Geltrú basins. A–
1235 D. *Sphaerochara ulmensis* from sample V6/7. A. apical view, IPS122528.1; B. lateral
1236 view, IPS122528.2; C. lateral views; IPS122528.3; D. basal view, IPS122528.4. E–I.
1237 *Sphaerochara ulmensis* from sample MA1, Mas de l’Alonso. E. apical view,
1238 IPS127516.1; F. lateral view, IPS127516.1; G. lateral view, IPS127516.2; H. lateral view,
1239 IPS127516.3; I. basal view, IPS127516.4; J–N. *Chara* cf. *vulgaris* from sample C4, els
1240 Casots. J. apical view, IPS127515.1; K. lateral view, IPS127515.2; L. lateral view,
1241 IPS127515.3; M. lateral view, IPS127515.4; N. basal view, IPS127515.5; O–R. *Chara*
1242 *molassica* var. *notata* from sample C4, els Casots. O. apical view, IPS127515.6; P. lateral
1243 view, IPS127515.7; Q. lateral view, IPS127515.8; R. basal view, IPS IPS127515.8; S–U.
1244 *Chara molassica* var. *notata* from sample V6/7, Vilobí del Penedès. S. apical view,
1245 IPS122528.5; T. lateral view, IPS122528.6; U. basal view, IPS122528.7

1246 Figure 7. Fossil charophyte assemblage from the Vallès-Penedès and Vilanova i la Geltrú
1247 basins (continued). A–H. *Chara* cf. *hispidia* from sample PG2. A. lateral view,
1248 IPS127517.1; B. lateral view, IPS127517.2; C. lateral view, IPS127517.3; D. lateral view,
1249 IPS127517.4; E. apical view, IPS127517.5; F. apical view, IPS127517.6; G. basal view,
1250 IPS127517.7; H. basal view, IPS127517.8; I–M. *Chara* sp. from sample PG2. I. apical
1251 view, IPS127517.9; J. lateral view, IPS127517.10; K. lateral view, IPS127517.11; L.
1252 lateral view, IPS127517.12; M. basal view, IPS127517.13; N–U. *Lamprothamnium*
1253 *papulosum* from sample V5, Vilobí del Penedès. N. lateral view, IPS127514.1; O. lateral
1254 view, IPS127514.2; P. lateral view, IPS127514.3; Q. lateral view, IPS127514.4; R. apical
1255 view, IPS127514.5; S. apical view, IPS127514.6; T. basal view, IPS127514.7; U. basal
1256 view, IPS127514.8.

1257 Figure 8. Fossil charophyte assemblage from the Vallès-Penedès and Vilanova i la Geltrú
1258 basins (continued). A–C. *Lychnothamnus barbatus* var. *antiquus* from sample V6/7,
1259 Vilobí del Penedès. A. apical view, IPS122528.8; B. lateral view, IPS122528.9; C. basal
1260 view, IPS122528.10; D–F. *Lychnothamnus* sp. from sample MA1, Mas de l'Alonso. D.
1261 apical view, IPS127516.5; E. lateral view, IPS127516.5; F. basal view, IPS127516.6; G–
1262 N. *Nitellopsis (Tectochara) merianii* from sample V6/7, Vilobí del Penedès. G. apical
1263 view, IPS122530.1; H. apical view, IPS122530.2; I. basal view, IPS122530.3; J. basal
1264 view, IPS122530.4; K. lateral view, IPS122530.5; L. lateral view, IPS122530.6; M.
1265 lateral view, IPS122530.7; N. lateral view, IPS122530.8; O–Q. *Nitellopsis* sp. from
1266 sample V6/7, Vilobí del Penedès. O. apical view, IPS122528.11; P. lateral view,
1267 IPS122528.11; Q. basal view. IPS122528.12.

1268 Figure 9. Fossil ostracods and foraminifera from Vallès-Penedès and Vilanova i la Geltrú
1269 basins. A–D. *Heterocypris salina* from sample PG2, el Pi Gros locality. A. external view
1270 of a right valve, IPS127517.14; B. internal view of a right valve, IPS127517.15; C. dorsal
1271 view of carapace, IPS127517.16; D. ventral view of carapace, IPS127517.17; E–J.
1272 ?*Leptocythere* gr. *L. psammophila* from sample PG2, el Pi Gros locality. E. external view
1273 of a left valve, IPS127517.18; F. external view of a left valve, IPS127517.19; G. external
1274 view of a right valve, IPS127517.20; H. opened carapaces from the ventral view,
1275 IPS127517.21; I. dorsal view of carapace, IPS127517.22; J. ventral view of carapace,
1276 IPS127517.23; K–M. *Ammonia* sp. from sample C4, els Casots. K. umbilical view,
1277 IPS127515.9; L. umbilical view, IPS127515.10; M. spiral view, IPS127515.11.

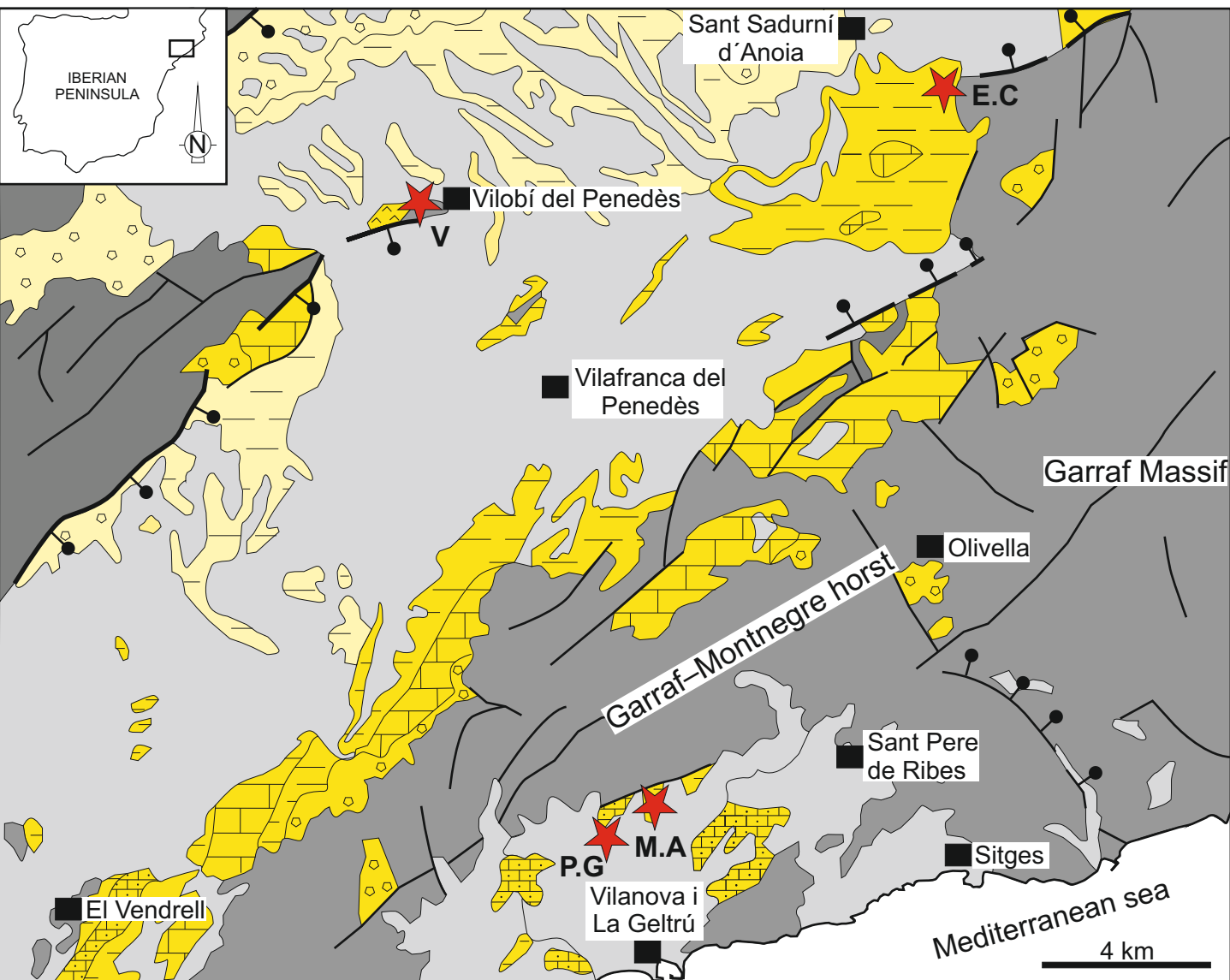
1278 Figure 10. Palaeoenvironmental model showing the distribution of the charophyte taxa
1279 and the distinguished depositional environments in the Vallès-Penedès and Vilanova i la
1280 Geltrú basins. Note that this is not a palaeoenvironmental reconstruction, as the Vallès-
1281 Penedès sites date back to the Langhian while those from the Vilanova i la Geltrú date

1282 back to the Serravallian. The figure is meant to illustrate the range of wetland
1283 environments occurring in these coastal basins during the Middle Miocene.

1284 Table 1. List of microfossils and their relative abundances based on a semi-quantitative
1285 visual estimation.

1286 Table 2 (in supplementary data). Biometric measurements of the studied charophyte
1287 samples from the Middle Miocene deposits of the E Vallès-Penedès and Vilanova i la
1288 Geltrú basins.

Figure 1

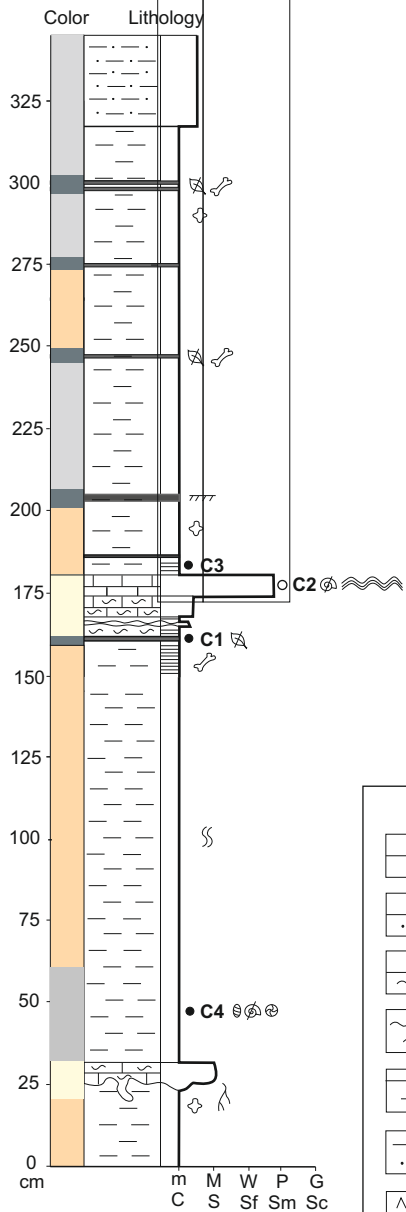


Legend

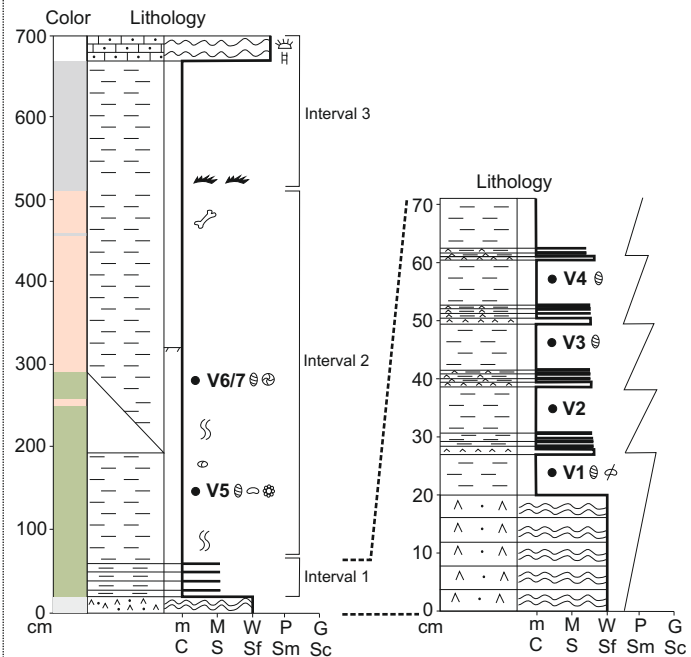
- | | | |
|------------------------|---|---|
| ■ Village | □ Quaternary (fluvial, alluvial and beach deposits) | □ Middle/Late Miocene (conglomerate) |
| ★ Section location | □ Early Miocene (conglomerate and coarse sandstone) | □ Middle/Late Miocene (marls and mudstone) |
| —● Major normal faults | □ Early Miocene (marls and mudstone) | □ Jurassic and Cretaceous rocks (limestone) |
| — Minor faults | □ Early Miocene (reefal limestone) | |
| | □ Early/Middle Miocene (bioclastic limestone) | |
| | □ Early Miocene (gypsum) | |

Figure 2

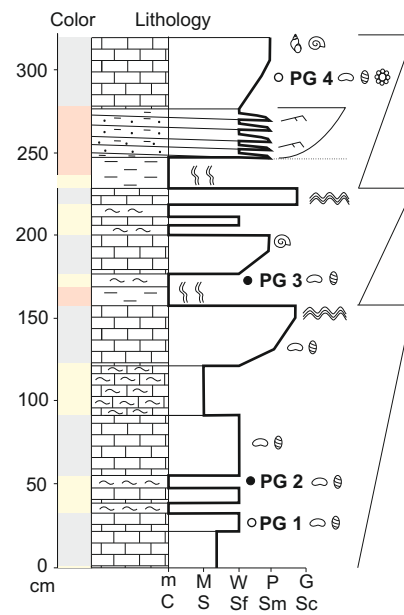
1. ELS CASOTS (SUBIRATS)



2. VILOBÍ DEL PENEDÈS



3. PI GROS (VILANOVA I LA GELTRÚ)



4. MAS DE L'ALONSO (VILANOVA I LA GELTRÚ)

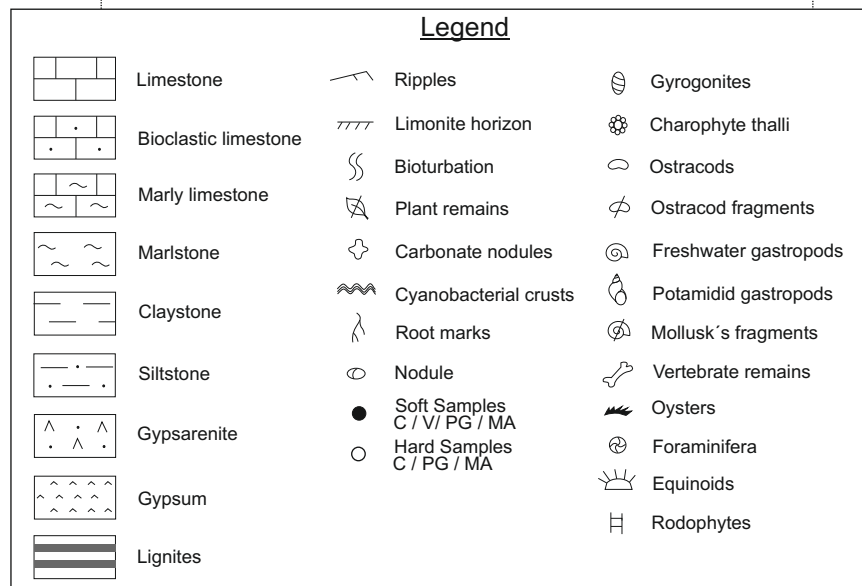
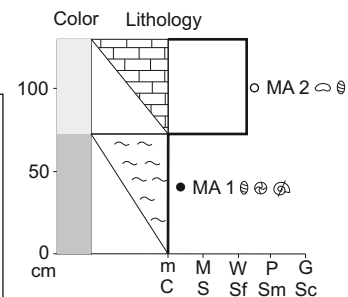


Figure 3

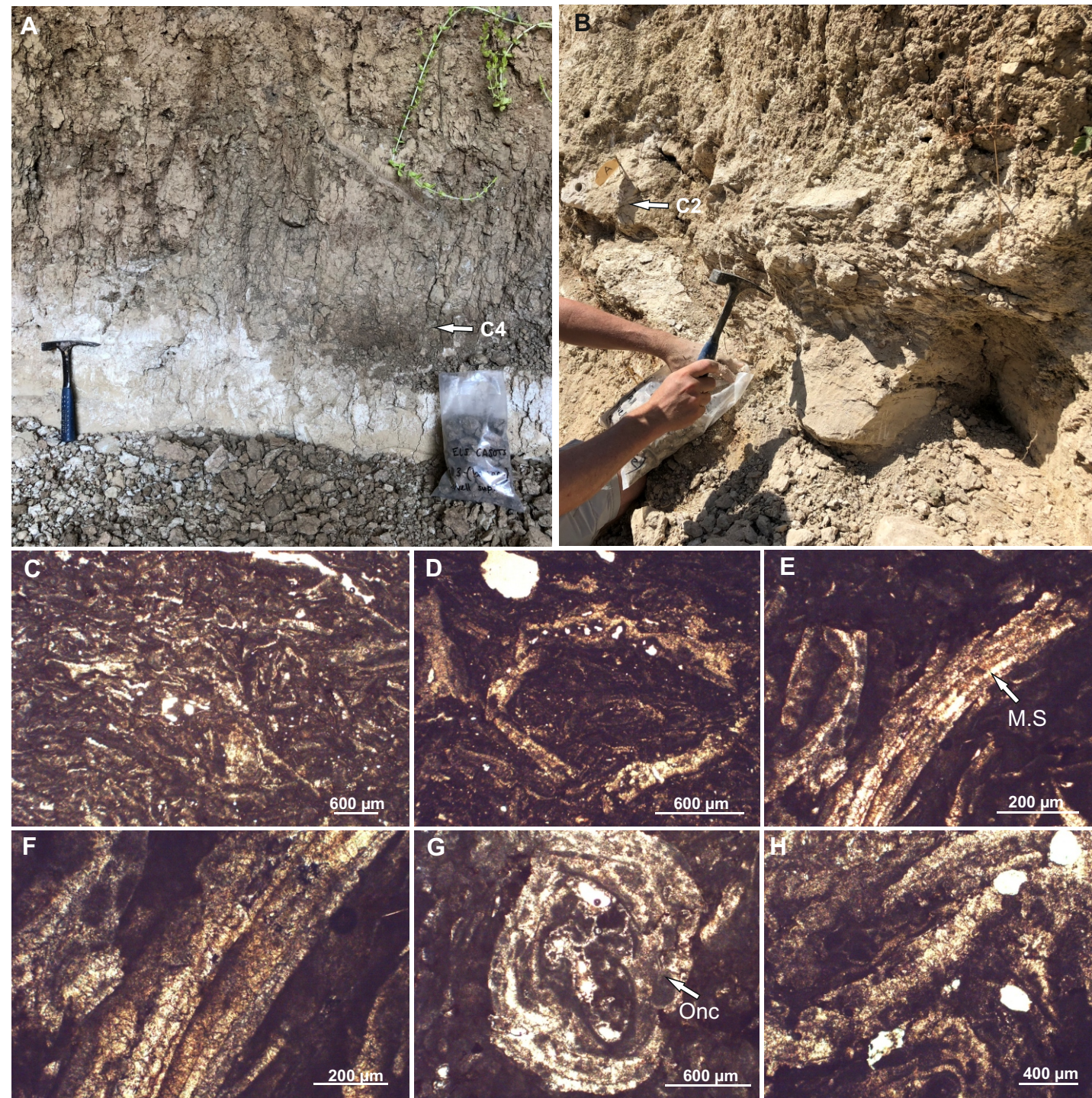


Figure 4

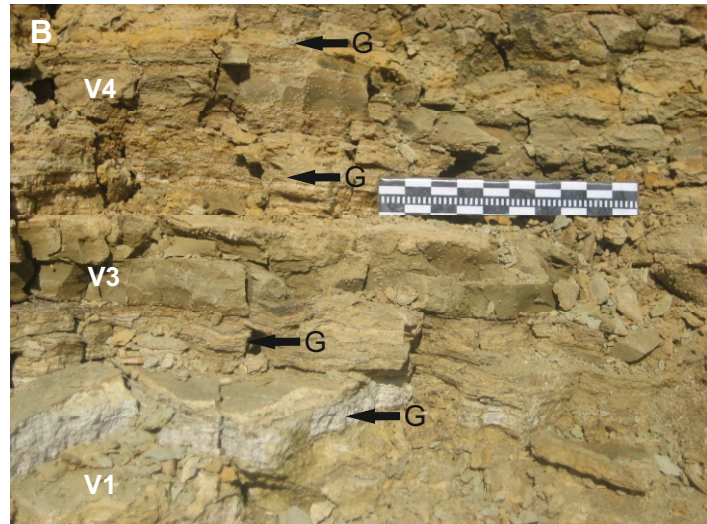


Figure 5

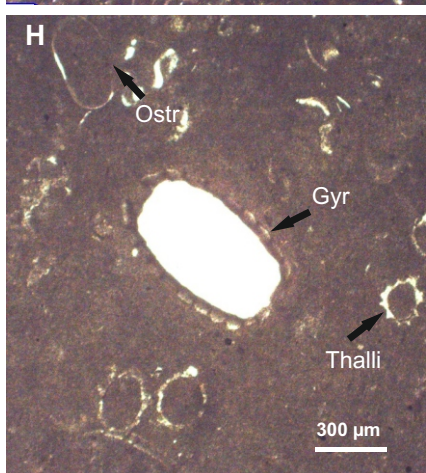
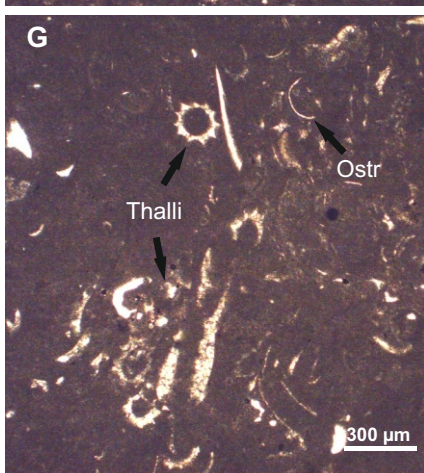
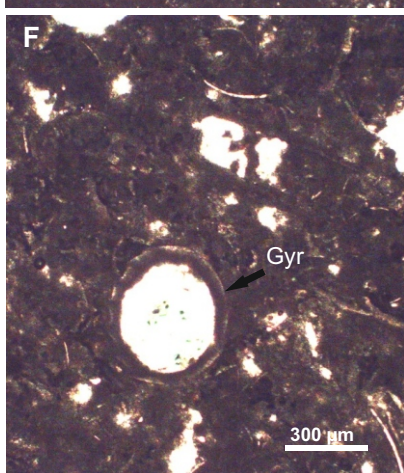
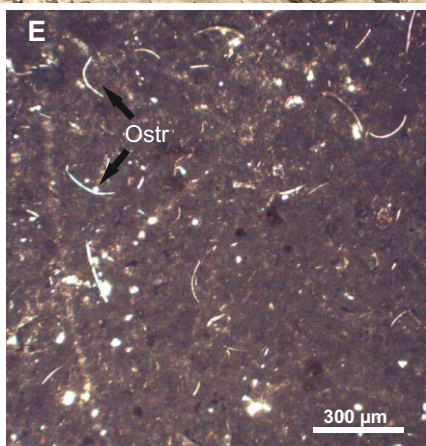
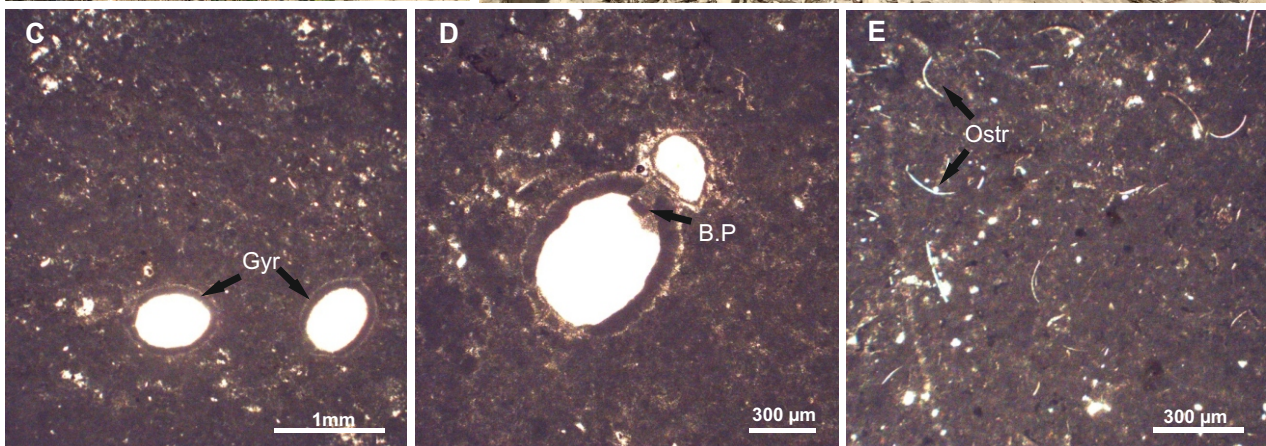
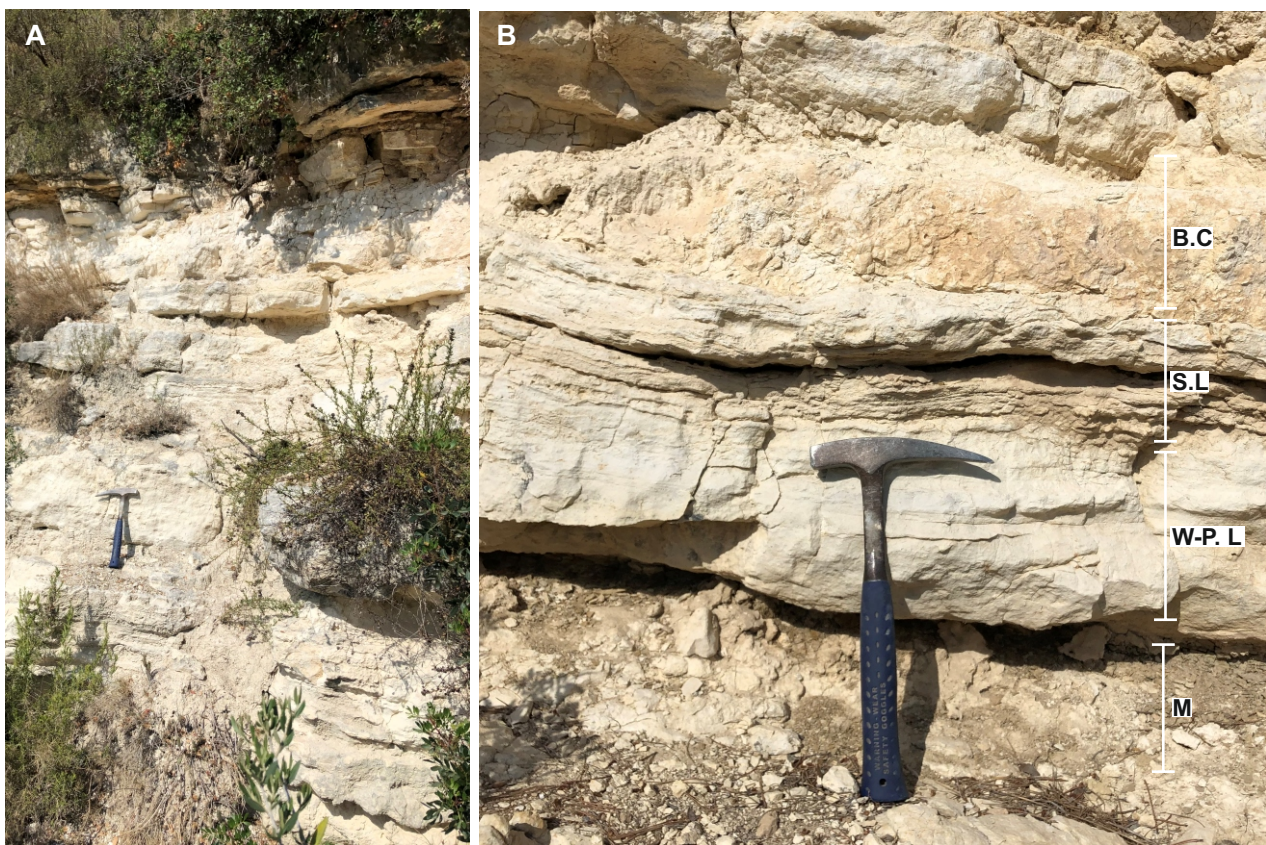


Figure 6

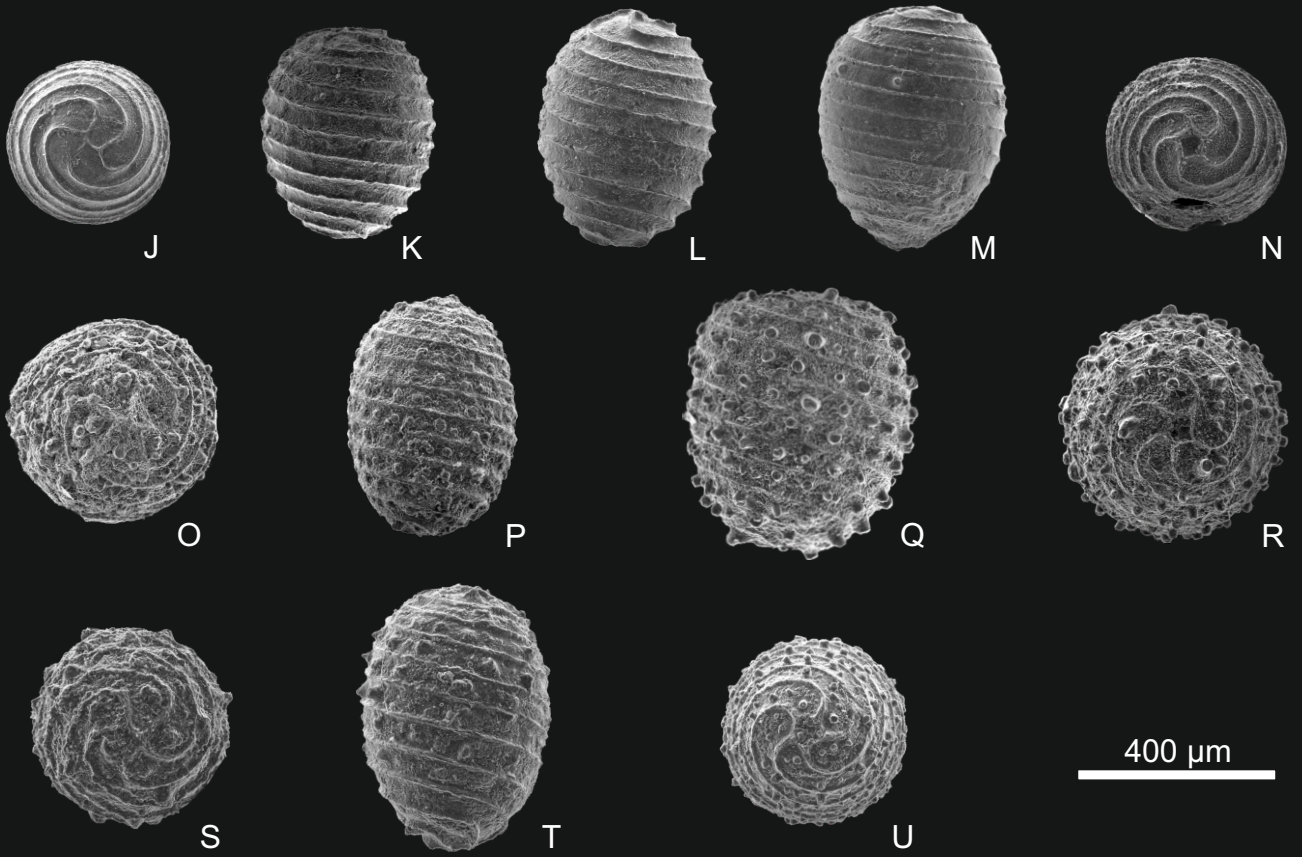
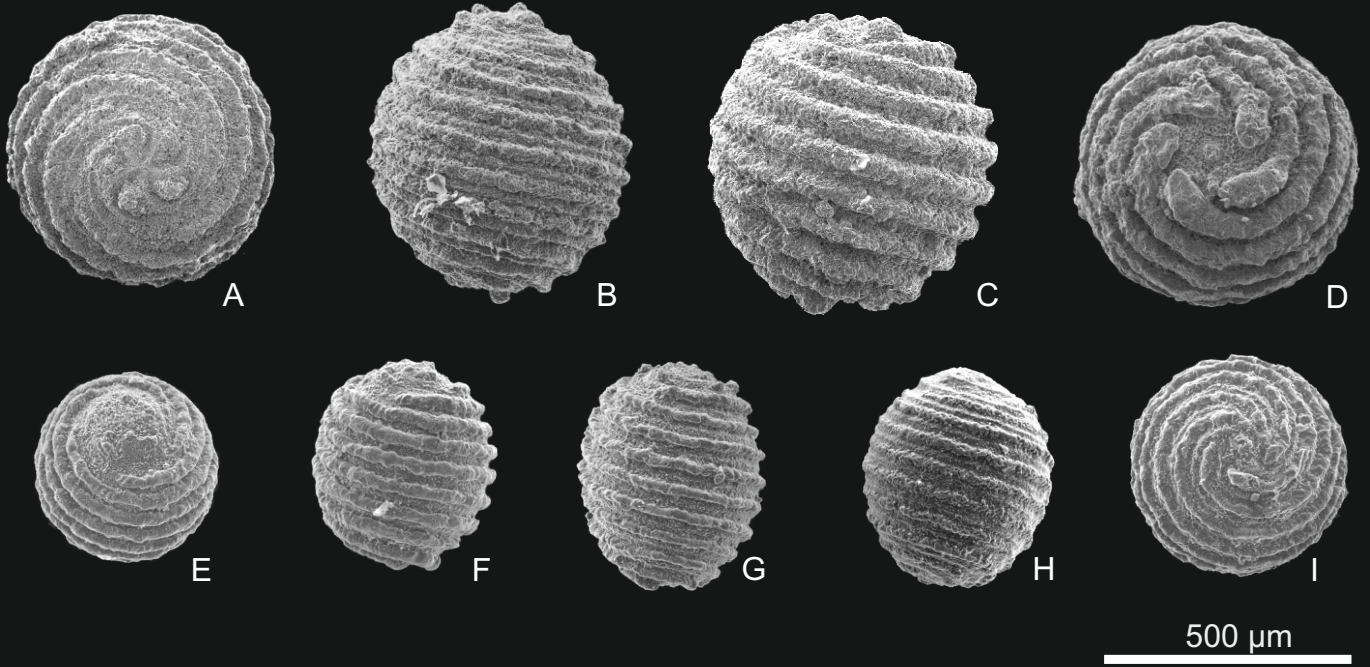


Figure 7

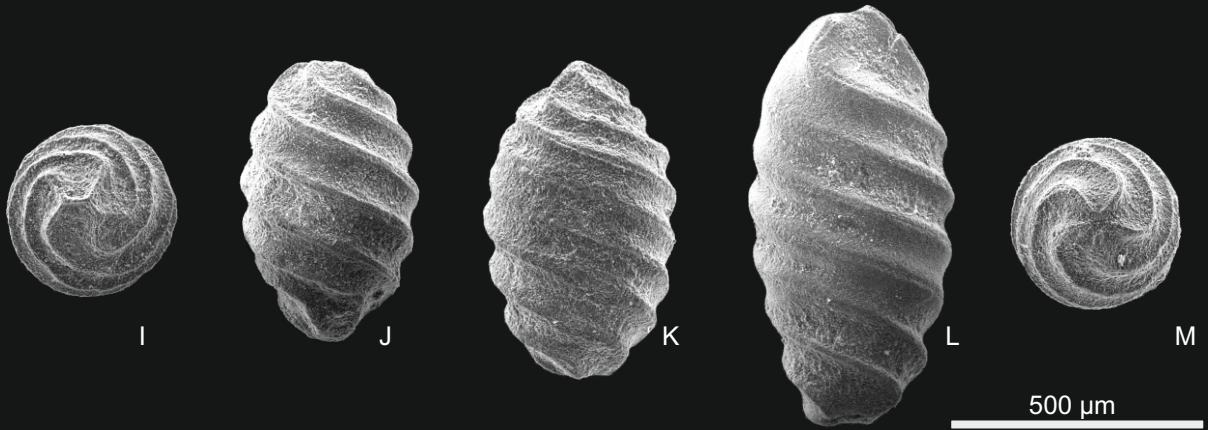
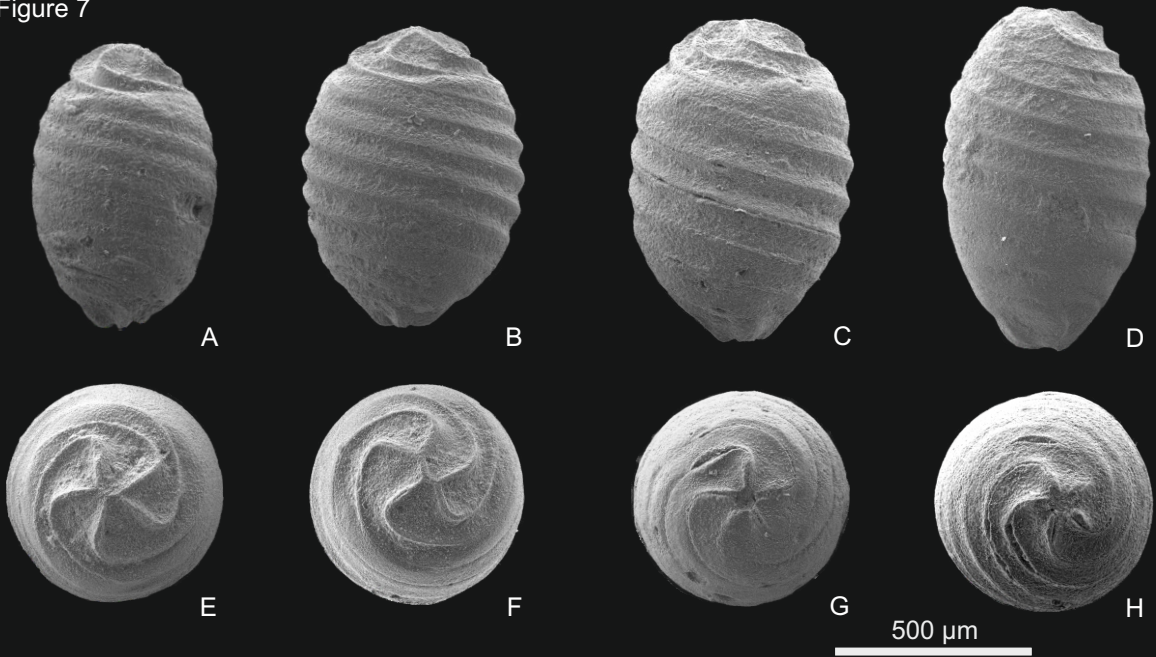


Figure 8

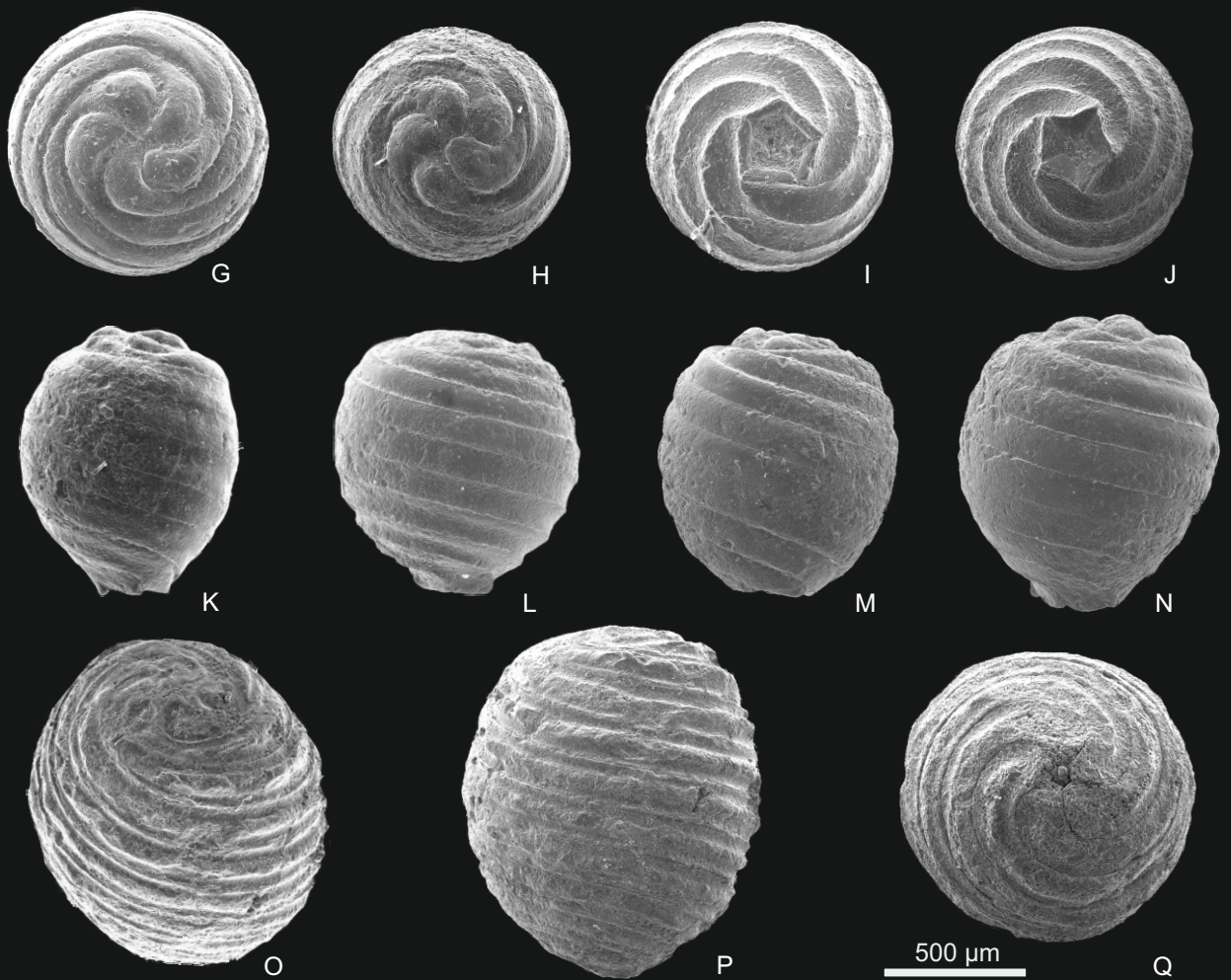
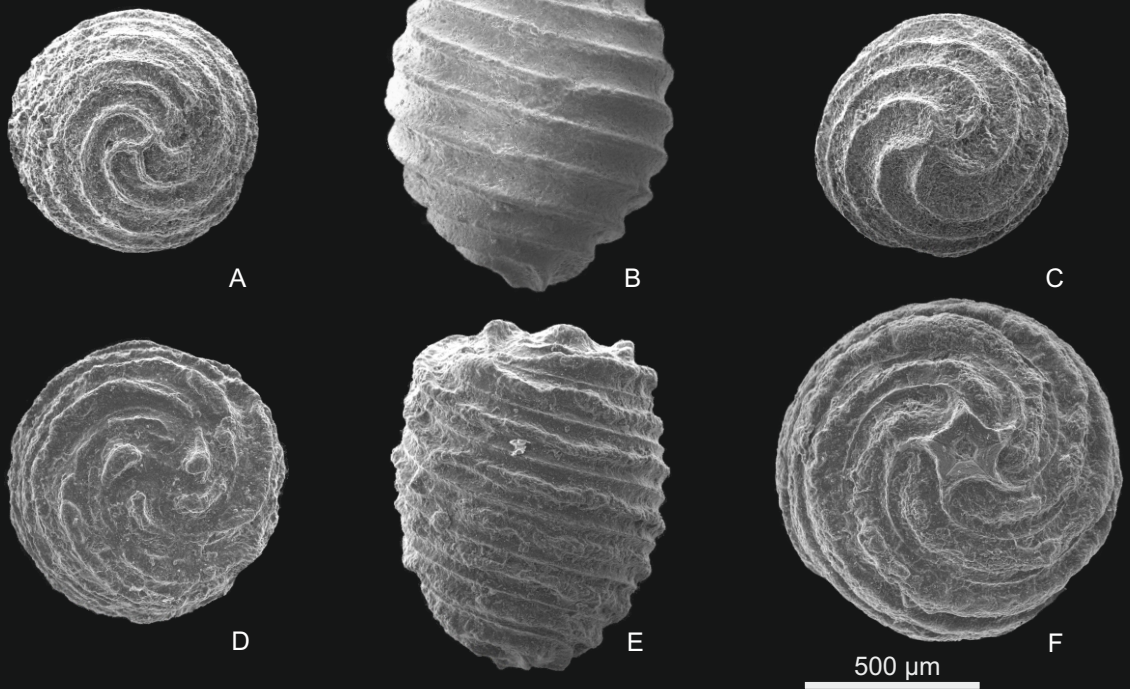


Figure 9

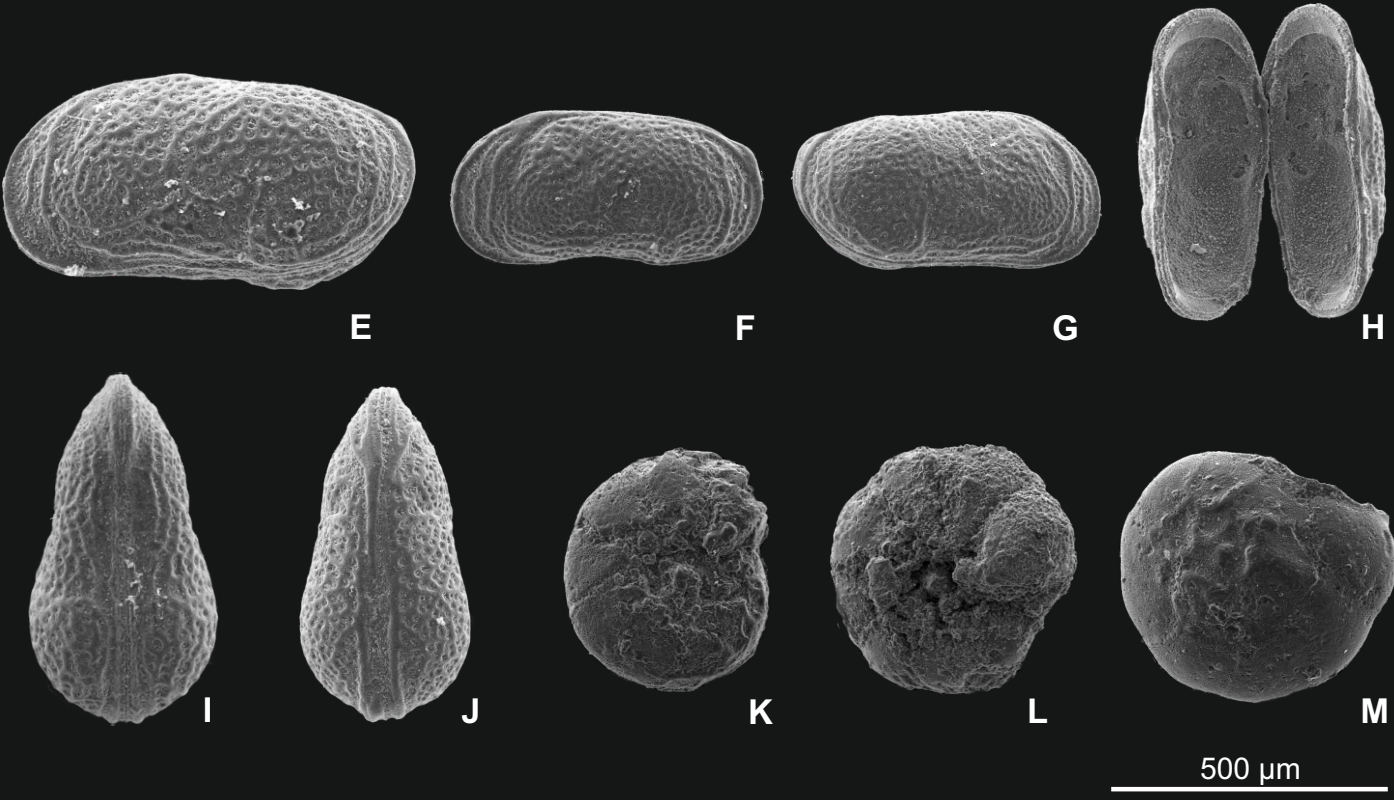
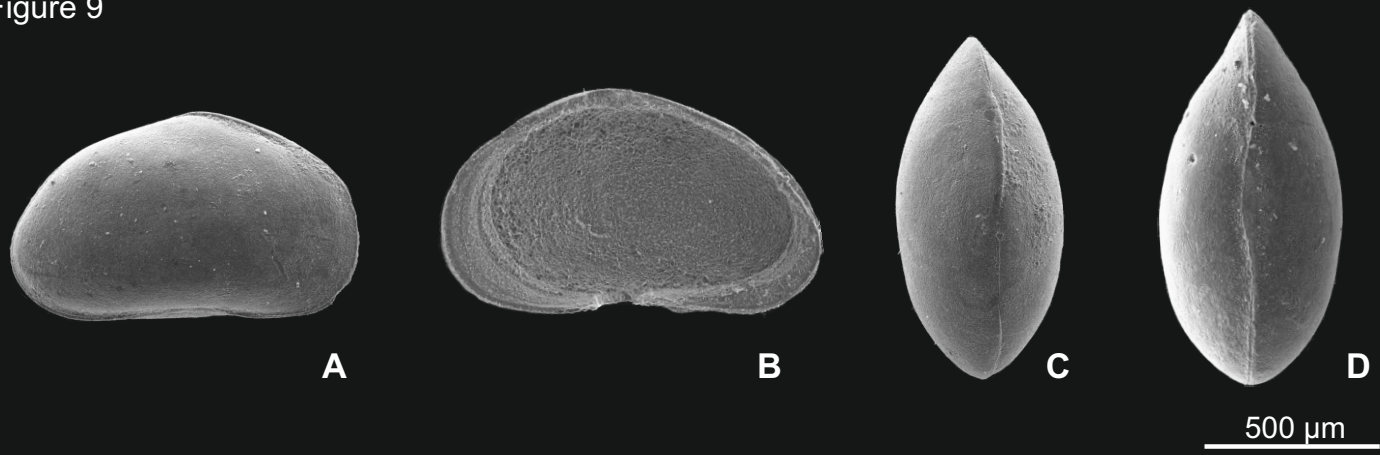
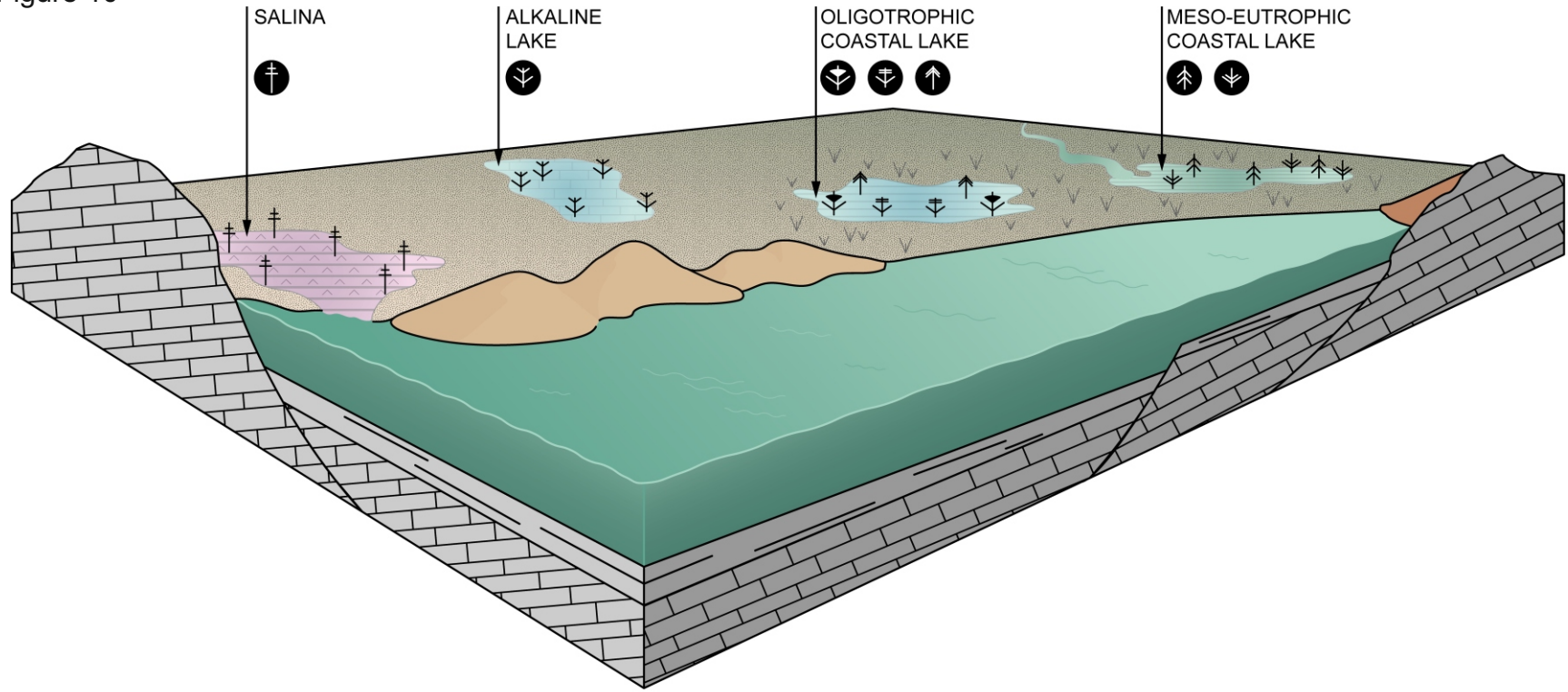


Figure 10



- ∇∇ Helophytic plants
- ‡ *Chara molassica* var. *notata*
- ∇ *Chara* cf. *hispida*
- ↑ *Lychnothamnus barbatus* var. *antiquus*
- † *Lamprothamnium papulosum*
- ∇ *Chara* cf. *vulgaris*
- ∇ *Sphaerochara ulmensis*
- ∇ *Nitellopsis merianii*

Table 1

Sample		Species	Charophytes										Ostracods	Foraminifera	Fish teeth	
			<i>Nitellopsis (T.) merianii</i>	<i>Nitellopsis</i> sp.	<i>Lychno. barbatus</i> var. <i>antiquus</i>	<i>Lychnothamnus</i> sp.	<i>Chara</i> cf. <i>vulgaris</i>	<i>Chara molassica</i> var. <i>notata</i>	<i>Chara</i> cf. <i>hispida</i>	<i>Chara</i> sp.	<i>Sphaerochara ulmensis</i>	<i>Lamprothamnium papulosum</i>	? <i>Leptocythere</i> gr. <i>psammophila</i>	<i>Heterocypris salina</i>	<i>Ammonia</i> sp.	indet.
El Pi Gros	PG 3							●	•			●	●			
	PG 2							●	•			●	●			
Mas de l'Alonso	MA 1	•			•			•		•				•	•	
Vilobí del Penedès	V 6/7	●	•	•			●			•				•		
	V 5										●					
	V 4										•					
	V 3										•					
	V 1										•					
els Casots	C 4					●	•							•	•	

Relative abundance • rare ● abundant ● rich

Table 2 (supplementary data).

H=gyrogonite height, μm
W=gyrogonite width, μm
C.N=convolution number in lateral view
S.C.H=spiral cell height, μm
ISI=Isopolarity index. $H/W \times 100$

ELS CASOTS

Chara molassica var. *notata*. Sample C4

H	W	C.N	S.C.H	ISI	
550	439	10	56	125	
491	369	11	44	133	
641	404	11	54	159	
538	418	11	44	129	
555	408	11	50	136	mean
491	369	10	44	125	min
641	439	11	56	159	max

Chara cf. *vulgaris*. Sample C4

H	W	C.N	S.C.H	ISI	
419	335	11	31	125	
475	375	12	53	127	
454	325	10	42	140	
501	305	10	33	164	
504	391	12	43	129	
520	365	11	38	142	
486	347	11	49	140	
435	386	10	53	113	
513	430	11	43	119	
483	359	10	42	135	
401	289	12	42	139	
455	371	11	52	123	
451	390	13	51	116	
552	359	11	38	154	
482	384	11	46	126	
460	402	11	44	114	
533	414	13	45	129	
529	429	12	49	123	
495	356	13	41	139	
473	357	11	49	132	
584	406	12	54	144	
446	360	11	41	124	
414	370	10	45	112	
437	355	11	37	123	
382	336	12	38	114	
468	374	11	44	125	

Table 2 (supplementary data).

456	293	12	40	156	
465	359	10	41	130	
481	375	10	54	128	
442	377	10	60	117	
470	299	10	48	157	
444	346	11	45	128	
456	333	10	39	137	
481	350	10	33	137	
474	301	11	42	157	
378	323	11	48	117	
435	345	12	43	126	
487	352	12	37	138	
468	323	11	48	145	
543	357	10	53	152	
492	330	10	57	149	
426	256	10	39	166	
449	325	12	40	138	
428	334	11	37	128	
386	319	10	39	121	
470	347	10	45	135	
467	361	12	46	129	
501	333	12	43	150	
419	325	10	42	129	
421	363	12	46	116	
466	352	11	44	133	mean
378	256	10	31	112	min
584	430	13	60	166	max

VILOBÍ DEL PENEDÈS

Chara molassica var. *notata*. Sample V6/7

H	W	C.N	S.C.H	ISI
488	320	11	53	153
570	402	11	56	142
542	383	10	68	142
517	331	9	60	156
498	411	10	52	121
544	389	9	71	140
531	368	10	51	144
557	384	9	72	145
547	368	11	51	149
468	333	10	58	141
523	386	10	57	135
478	398	10	64	120
509	344	9	60	148
558	367	10	50	152
451	416	8	69	108

Table 2 (supplementary data).

599	407	10	60	147	
508	375	9	59	135	
513	412	8	53	125	
438	336	10	51	130	
519	407	10	61	128	
527	398	9	69	132	
580	363	11	46	160	
513	407	9	52	126	
480	353	10	47	136	
551	415	9	69	133	
536	401	9	61	134	
452	343	9	66	132	
491	347	10	54	141	
527	375	11	57	141	
584	362	12	51	161	
517	396	9	69	131	
520	377	10	59	138	mean
599	416	12	72	161	max
438	320	8	46	108	min

Sphaerochara ulmensis. Sample V6/7

H	W	C.N	S.C.H	ISI	
590	576	10	62	102	
630	619	9	73	102	
652	564	9	84	116	
623	569	9	74	109	
596	582	9	79	102	
622	567	10	73	110	
614	514	10	64	119	
571	514	10	63	111	
607	578	10	71	105	
612	565	10	71	109	mean
652	619	10	84	119	max
571	514	9	62	102	min

Nitellopsis (Tectochara) merianii. Sample V6/7

H	W	number conv.	conv H	ISI	
986	863	9	130	114	
964	856	9	161	113	
969	790	8	149	123	
1035	767	9	130	135	
907	832	8	145	109	
781	656	8	104	119	
914	774	8	170	118	
1004	786	7	158	128	
1120	957	8	171	117	

Table 2 (supplementary data).

997	818	7	183	122	
998	856	7	145	117	
1079	914	8	141	118	
947	867	8	149	109	
922	886	7	179	104	
933	852	7	158	110	
843	786	9	107	107	
894	810	7	137	110	
958	866	8	130	111	
1023	815	7	123	126	
804	676	7	104	119	
955	811	7	158	118	
854	709	7	118	120	
959	847	7	131	113	
1036	904	8	131	115	
1066	913	9	181	117	
1004	865	8	152	116	
899	816	7	130	110	
943	813	7	164	116	
988	838	7	139	118	
928	697	7	131	133	
951	878	9	114	108	
1060	914	9	134	116	
914	841	8	129	109	
981	836	9	122	117	
900	740	8	140	122	
958	824	8	141	116	mean
1120	957	9	183	135	max
781	656	7	104	104	min

Nitellopsis sp. Sample V6/7

H	W	C.N	S.C.H	ISI	
1335	1053	8	164	127	
1243	1048	9	146	119	
1289	1051	9	155	123	mean

Lychnothamnus barbatus var. *antiquus*. Sample V6/7

H	W	C.N	S.C.H	ISI	
934	787	10	113	119	
726	600	9	107	121	
974	812	10	153	120	
878	733	10	124	120	mean

Lamprothamnium papulosum. Sample V5

H	W	C.N	S.C.H	ISI	
592	464	10	88	128	

Table 2 (supplementary data).

639	506	10	85	126
583	491	9	85	119
700	486	11	70	144
632	504	10	75	125
653	490	10	85	133
608	460	10	63	132
663	542	11	78	122
638	495	11	85	129
634	459	10	86	138
613	488	11	85	126
653	484	10	82	135
598	446	11	68	134
581	486	10	68	120
638	499	9	87	128
627	442	10	73	142
658	455	10	67	145
591	458	9	78	129
650	507	9	73	128
583	478	9	94	122
569	431	9	87	132
639	455	10	88	140
604	479	9	89	126
628	528	9	76	119
657	422	8	100	156
666	452	8	73	147
606	460	8	76	132
610	538	8	93	113
651	499	9	84	130
640	460	9	96	139
619	478	9	87	129
649	505	9	95	129
617	467	9	89	132
639	457	8	85	140
637	510	8	70	125
636	447	8	85	142
625	444	8	71	141
589	441	9	95	134
620	484	10	92	128
586	422	9	87	139
591	413	8	85	143
629	433	9	67	145
690	436	9	72	158
610	455	9	75	134
616	462	11	76	133
599	460	9	78	130
663	373	9	73	178

Table 2 (supplementary data).

631	511	10	90	123	
661	448	8	75	148	
638	501	9	84	127	
601	474	8	89	127	
571	391	8	95	146	
649	506	10	62	128	
677	459	9	73	147	
622	459	9	78	136	
701	528	9	81	133	
682	519	8	86	131	
711	452	9	86	157	
682	480	9	96	142	
585	348	8	75	168	
631	469	9	81	135	mean
711	542	11	100	178	max
569	348	8	62	113	min

MAS DE L'ALONSO-EL PI GROS

Chara cf. hispida. Sample PG2

H	W	C.N	S.C.H	ISI
783	540	10	80	145
783	540	9	88	145
783	513	10	104	153
783	540	10	88	145
783	567	9		138
567	378	8		150
810	540	10		150
621	432	10		144
621	459	9		135
810	540	10		150
864	567	8		152
594	378	8		157
783	540	10		145
756	486	9		156
810	567	10		143
810	540	11		150
648	405	10		160
540	432	12		125
594	405			147
810	567			143
675	351			192
810	540			150
756	567			133
729	540			135
756	540			140
729	513			142

Table 2 (supplementary data).

729	513	142
756	540	140
540	405	133
783	540	145
810	567	143
675	486	139
648	405	160
702	540	130
810	540	150
702	432	163
891	439	203
648	567	114
675	540	125
540	432	125
648	432	150
810	540	150
567	405	140
702	567	124
724	540	134
756	513	147
702	432	163
756	513	147
648	405	160
837	540	155
783	540	145
702	486	144
756	459	165
783	486	161
675	513	132
810	567	143
783	540	145
783	540	145
648	405	160
621	405	153
702	486	144
810	567	143
756	513	147
540	351	154
783	540	145
702	486	144
594	540	110
783	567	138
810	513	158
810	513	158
621	486	128
756	459	165

Table 2 (supplementary data).

594	432				138
756	513				147
567	432				131
594	405				147
837	405				207
810	621				130
756	486				156
783	567				138
687	540				127
756	486				156
729	486				150
729	513				142
702	540				130
810	540				150
702	540				130
783	567				138
540	378				143
675	540				125
810	540				150
810	540				150
729	540				135
621	486				128
756	540				140
810	459				176
726	467				155
774	548				141
806	572				141
854	516				166
726	500	9,6	90	145	mean
891	621			207	max
540	351			110	min

Chara sp. Sample PG2

H	W	C.N	S.C.H	ISI	
612	350	6	100	175	
625	387	7	75	161	
825	400	7	112	206	
687	379	7	96	181	mean

Sphaerochara ulmensis. Sample MA1

H	W	C.N	S.C.H	ISI	
477	431	9	50	111	
433	407	10	41	106	
413	330	10	39	125	
413	378	9	43	109	
446	385	10	43	116	

Table 2 (supplementary data).

398	374	9	53	106	
447	379	9	44	118	
447	363	9	54	123	
449	409	10	61	110	
446	410	10	52	109	
418	375	10	43	111	
447	421	10	66	106	
442	404	9	45	109	
426	383	9	60	111	
466	402	9	53	116	
460	417	9	57	110	
410	388	9	62	106	
437	397	10	48	110	
424	402	10	57	105	
436	406	9	63	107	
421	375	9	62	112	
453	378	10	54	120	
437	390	9	51	112	
437	391	9	52	112	mean
477	431	10	66	125	max
398	330	9	39	105	min

Lychnothamnus sp. Sample MA1

H	W	C.N	S.C.H	ISI
1022	777	8	70	131